applied mechanics

MDPI

Article

A Deterministic Methodology to Calibrate Pressure-Independent Anisotropic Yield Criteria in Plane Strain Tension Using Finite-Element Analysis

A. Abedini *, A. Narayanan and C. Butcher

Department of Mechanical and Mechatronics Engineering, University of Waterloo, Waterloo, ON N2L 3G1, Canada; anadvait@uwaterloo.ca (A.N.); cbutcher@uwaterloo.ca (C.B.)
* Correspondence: aabedini@uwaterloo.ca

Abstract: The yield strength of materials under plane strain deformation is often not characterized experimentally due to difficulties that arise in interpreting the results of plane strain tensile tests. The strain and stress fields in the gauge region of these tests are inhomogeneous, making it challenging to extract the constitutive response from experimental measurements. Consequently, the plane strain yield stress is instead predicted using phenomenological plasticity models calibrated using uniaxial and biaxial tension data. To remove this uncertainty, a simple finite-element based inverse technique is proposed to determine the arc of the associated yield *locus* from uniaxial-to-plane strain tension using a constrained form of Vegter's anisotropic yield criterion to analyze a notch tensile test. The inverse problem is formulated under associated deviatoric plasticity and constrained such that only a single parameter, the major principal yield stress under plane strain deformation, needs to be identified from the finite-element simulations. The methodology was applied to two different automotive steel grades, an ultra-high strength DP1180 and a DC04 mild steel. The predictive accuracy of the constitutive models was then evaluated using an alternate notch geometry that provides an intermediate stress state between uniaxial and plane strain tension. By performing notch tensile tests in three sheet orientations, three arcs of the yield surface were obtained and employed to calibrate the widely used Yld2000 yield function. The study shows that for DP1180, the normalized plane strain yield stress was in the range of 1.10 to 1.14 whereas for DDQ steel, the normalized plane strain yield stress was notably stronger, with values ranging from 1.22 to 1.27, depending on the orientation. The proposed methodology allows for a wealth of anisotropic plasticity data to be obtained from simple notch tests while ensuring the plane strain state is accurately characterized, since it governs localization and fracture in many forming operations.

Keywords: plane strain loading; anisotropic yield function; constitutive response; dual-phase steel; mild steel; inverse analysis; notch tension test

Citation: Abedini, A.; Narayanan, A.; Butcher, C. A Deterministic Methodology to Calibrate Pressure-Independent Anisotropic Yield Criteria in Plane Strain Tension Using Finite-Element Analysis. *Appl. Mech.* **2022**, *3*, 905–934. https://doi.org/10.3390/applmech3030052

Received: 13 May 2022
Accepted: 25 July 2022
Published: 28 July 2022

1. Introduction

Understanding the plastic response of materials under plane strain deformation is critical to the design of sheet metal forming operations. Under tensile-dominant loading conditions, deformation is homogeneous until the onset of necking, after which the stress state transitions to plane strain tension, followed by fracture. The strains to initiate localization and fracture are typically the lowest under plane strain tension, hence, this mode of deformation is often considered as the most critical state in sheet metal forming operations [1,2]. From an analytical perspective, the magnitude of the major stress in plane strain tension is an extremum point on the yield surface that should be properly calibrated to accurately predict the material response in forming and crash simulations. Despite the importance of the plane strain state, this mode of deformation is often overlooked in phenomenological plasticity, with the plane strain region not directly characterized and, instead, predicted, based upon uniaxial and equal biaxial tensile data.

The so-called "conventional approach" to the calibration of anisotropic constitutive models using uniaxial and equal biaxial tensile data has been widely adopted because reliable experimental constitutive data in plane strain tension is often not available. Among the experimental techniques targeting plane strain characterization (such as notch tension, elliptical bulge, cruciform, and plane strain compression tests), notched tensile tests are the most popular, owing to their simplicity with numerous geometries proposed in the literature [3–8]. Regardless of the geometry of the plane strain notch specimen, there are unavoidable stress/strain gradients that develop across the gauge width of the specimens. Deformation is plane strain tension near the center of the gauge area, and transitions to uniaxial tension at the edge or notch root. The inevitable non-uniform deformation field makes it challenging to directly extract the plane strain stress-strain response from the test data. Approximations have been proposed to correct the stress-strain curves by introducing scale factors that are typically derived based on finite-element analysis assuming the quadratic von Mises criterion [5,7,8]. These isotropic scale factors are then applied to anisotropic materials where the error due to the inconsistent modeling procedure depends upon the degree of anisotropy of the material.

As discussed by Butcher and Abedini [9], it is typically assumed that the stress state (or the principal stress ratio) is unknown in plane strain tension and must be derived from a phenomenological yield criterion after the conventional calibration of its parameters. Therefore, both the magnitudes of principal stresses under plane strain deformation and their locations on the yield *locus* are taken as unknowns to be determined as a by-product of the calibration using tensile and equal biaxial data. This approach holds for pressure-dependent plasticity where the plane strain extrema are unknown, but not for associated pressure-independent (deviatoric) plasticity, which is commonly adopted to describe the anisotropic behavior of sheet metals. In associated deviatoric plasticity, a non-zero plastic strain increment requires a non-zero deviatoric stress, and vice versa. In plane stress, this corresponds to the principal stress ratio of $\frac{\sigma_2}{\sigma_1} = 0.5$, such that the minor deviatoric stress is zero, $s_2 = 0$, for there to be no increment in the plastic strain or $d\varepsilon_2^p = 0$. This condition is not automatically fulfilled in phenomenological anisotropic yield functions that are based on linear transformations on the deviatoric stress tensor. Consequently, the authors proposed the "generalized plane strain constraint" that should be enforced upon the principal normal vectors in the calibration of yield criteria, such as the Barlat family of anisotropic yield criteria [10–12]. Recently, Fast-Irvine et al. [13] strictly enforced the plane strain constraints on the anisotropic Hosford yield function [14] and employed a cutting line approach for a notch specimen using Digital Image Correlation (DIC) strain measurements to inversely determine the yield exponent. Fast-Irvine et al. [13] demonstrated that only the major stress in plane strain deformation needs to be identified and, consequently, the inverse problem to calibrate the anisotropic yield function can be formulated in a deterministic manner.

Inverse finite-element analysis in conjunction with experiments to determine plasticity model parameters have become more popular with advancements in full-field DIC techniques. In this methodology, the experiment is simulated by iteratively updating the material model parameters. The procedure is terminated when the difference between model predictions and experimentally measured data (such as load-displacement, strain field, temperature field, etc.) is minimized. This technique has been utilized in the literature to primarily obtain the equivalent stress-strain or hardening response of materials to large strains assuming the yield function parameters are known *a priori* [15–19]. Nonetheless, the shape of the adopted yield surface can potentially have a strong impact on the resolved hardening curves (see, for instance, Ha et al. [18]) which introduces calibration bias. The hardening response of a material is an intrinsic material property and, thus, the inverse approach becomes problematic, especially if the plane strain yield strength was not independently verified but predicted from the assumed yield function.

With recent advances in developing robust experimental techniques that use DIC strain measurements to derive hardening behavior of materials to strain levels much higher than uniform strain in a tensile test (Abedini et al. [20]), the focus of the inverse analysis can be directed towards obtaining the yield function shape, particularly at locations where experimental data is not readily available, such as in the plane strain regions. Recently, the authors proposed an inverse approach based on the Yld91 criterion [10] and a notch tensile test to estimate yield strength of sheet metals in plane strain tension (Narayanan et al. [21]). It was discussed by Narayanan et al. [21] that, due to the shape of the notch specimens, a non-trivial in-plane plane shear stress may develop in the gauge region of the specimen that can activate tensile loading in different orientations. While the approach of Narayanan et al. [21] is promising, a more user-friendly methodology is required to consider all material directions in the inverse analysis, which can be adopted by industry for enhanced calibration of anisotropic yield surfaces.

The goal of the present study was to develop a straightforward deterministic approach to determine the constitutive behavior of anisotropic sheet metals in plane strain using notched tension tests and inverse finite-element modeling. To this end, a constrained form of the anisotropic Vegter yield criterion [22] was employed. Unlike other advanced anisotropic yield criteria, the parameters of the Vegter model are determined directly from experiments, rather than through complex regression analysis. The major principal yield stress under plane strain deformation can be treated as a variable to control the local shape of the yield *locus* in the plane strain zone. The hardening response and R-value are obtained from tensile tests and the inverse analysis is limited to the uniform tensile elongation to avoid any artefacts arising from the hardening extrapolation or evolving R-values. The inverse problem under associated deviatoric plasticity is developed in accordance with mechanics of plane strain deformation and is fully constrained, such that only the major principal yield stress in plane strain needs to be determined from correlation of the measured and predicted force-displacement response from plane strain notch tension tests and simulations. The technique was applied to two different automotive rolled steel sheets with significant contrasts in their mechanical properties: an advanced high strength steel, DP1180, and a deep-draw quality (DDQ) DC04 mild steel. To evaluate the transferability of the yield function calibration, an alternate notch geometry was considered to provide an intermediate stress state between uniaxial and plane strain. The advantage of the proposed methodology is that, with only uniaxial tensile and plane strain notch tests, the entire arc of the associated yield function from uniaxial to plane strain tension can be characterized. Due to the widespread industrial use of the Barlat-family of yield criteria, the Yld2000 [11] yield criterion was adopted as an alternate yield function and calibrated for both materials using results of the inverse finite-element analysis with the Vegter model.

2. Materials and Experiments

Two different automotive steel sheets were studied: a high-strength dual-phase DP1180 steel with a nominal thickness of 1.0 mm, and a 2.0 mm thick DC04 mild steel with deep-draw quality (DDQ). Throughout the paper, the two materials are referred to as DP1180 and DDQ, respectively. The two steels were characterized under various stress states covering uniaxial tension stress-strain and R-values in seven (DP1180) or five (DDQ) orientations, simple shear in three directions, and the equal biaxial R-value. All the tests were performed at room temperature (23 °C) with a quasi-static strain rate of 0.001 s^{-1} with at least 3–5 repeats performed per condition to ensure repeatability. A detailed description of anisotropy characterization of DP1180 can be found in Abedini et al. [23] and the same procedure was adopted to characterize the DDQ steel. This available database allowed the present study to focus on anisotropy characterization under plane strain deformation. Table 1 summarizes the experimental data for the two materials and Figure 1 depicts the engineering stress-strain responses for representative repeats in the rolling or 0° (RD), diagonal or 45° (DD), and transverse or 90° (TD) orientations obtained with a standard tensile specimen.

Table 1. Experimentally characterized R-values (R) and yield stresses in tension (σ) and shear (τ) normalized with respect to tensile stress in the RD. The subscript indicates the orientation (in degrees) of the major principal direction with respect to the rolling direction of the sheets. The values provided in brackets present the standard deviations. The variable w^p is the plastic work per unit volume that was selected based on the tensile orientation with the lowest necking strain and was the plastic work at the start of diffuse necking for DP1180, and half of the plastic work at diffuse necking for DDQ to reduce potential distortional hardening effects.

Material	DP1180	DDQ
w^p [MJ/m^3]	61.11	34.76
σ_0/σ_0	1.000 (0.006)	1.000 (0.006)
σ_{15}/σ_0	0.995 (0.003)	-
$\sigma_{22.5}/\sigma_0$	-	1.024 (0.007)
σ_{30}/σ_0	0.996 (0.003)	-
σ_{45}/σ_0	1.004 (0.007)	1.042 (0.008)
σ_{60}/σ_0	1.008 (0.008)	-
$\sigma_{67.5}/\sigma_0$	-	1.019 (0.007)
σ_{75}/σ_0	1.013 (0.003)	-
σ_{90}/σ_0	1.025 (0.007)	0.992 (0.008)
τ_0/σ_0	0.600 (0.005)	0.571 (0.010)
$\tau_{22.5}/\sigma_0$	0.600 (0.008)	0.595 (0.021)
τ_{45}/σ_0	0.612 (0.005)	0.607 (0.009)
R_0	0.82 (0.01)	2.09 (0.04)
R_{15}	0.84 (0.01)	-
$R_{22.5}$	-	1.82 (0.03)
R_{30}	0.90 (0.01)	-
R_{45}	0.95 (0.01)	1.55 (0.03)
R_{60}	0.98 (0.01)	-
$R_{67.5}$	-	1.98 (0.04)
R_{75}	1.00 (0.00)	-
R_{90}	0.98 (0.01)	2.46 (0.04)
R_b	0.94 (0.03)	0.85 (0.03)

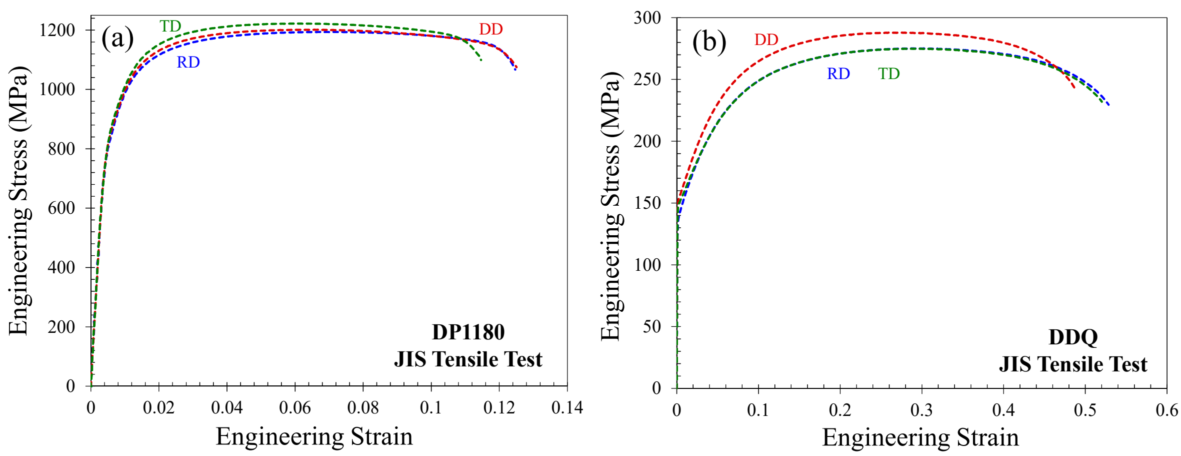

Figure 1. Engineering stress-strain response of (**a**) DP1180, and (**b**) DDQ steel sheets determined in three orientations of RD, DD, and TD using a JIS No.5 standard tensile specimen at a strain rate of 0.001 s^{-1}.

Notch tensile tests were conducted in the present study by adopting the specimen geometries shown in Figure 2a,b in three different directions with respect to the rolling direction of the sheets (RD, DD, and TD). The sample geometry in Figure 2a is referred to as the "plane strain notch" geometry and was selected since it has a simple design and can facilitate achieving plane strain deformation in the center of the gauge region. In addition, the small gauge width of the specimen induces strong in-plane stress and strain gradients to promote fracture at the gauge center. A methodology to determine plane strain regions of anisotropic yield criteria was developed based on this geometry. The so-called "NT20" specimen geometry in Figure 2b was adopted from Roth and Mohr [24] and is considered as an *assessment test* that can activate stress states between uniaxial and plane strain tension. To report global deformation in terms of far-field strains, gauge lengths of 16 mm and 35 mm were selected for plane strain notch and NT20 specimens, respectively (depicted in Figure 2a). Experiments were conducted using standard tensile frames with cross-head velocities of 0.005 mm/s and 0.030 mm/s for the plane strain notch and NT20 specimens, respectively. Figure 3 depicts the test setup and the notched specimens before and after the experiments.

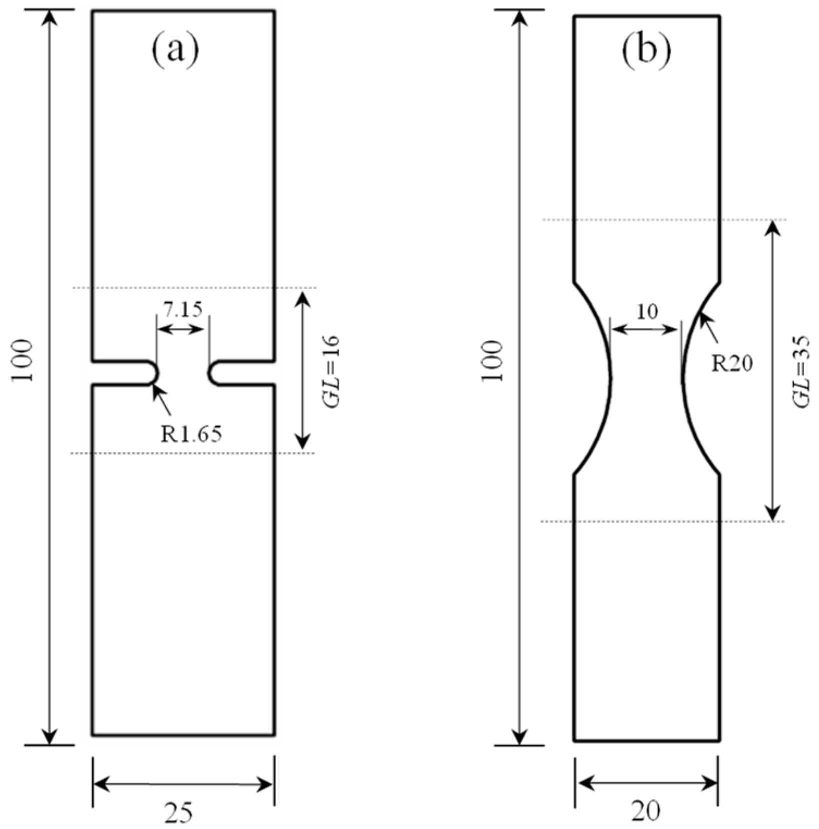

Figure 2. Geometries of (**a**) plane strain notch specimen, and (**b**) NT20 notch specimen of Roth and Mohr (2016). All dimensions are in millimeters and *GL* stands for "gauge length" selected to report far-field elongation.

For all the tests, full-field stereoscopic DIC techniques were employed to measure strains. The DIC images were captured with a prescribed frequency such that a minimum of 300 images were taken from the onset of deformation until fracture. The Vic-3D software from Correlated Solutions, Inc. was used for DIC analysis. For consistency, a virtual strain gauge length (*VSG*, with the definition given in Equation (1)) equal to the initial sheet thickness was used for DIC analysis, with the corresponding parameters listed in Table 2.

$$VSG[\text{mm}] = (\text{step size [pixel]} \times (\text{filter size} - 1) + \text{subset size[pixels]}) \times \text{resolution [mm/pixel]} \quad (1)$$

Table 2. DIC parameters used for strain measurements.

Test	Material	Test Direction	Image Resolution (mm/pixel)	Step Size (pixel)	Filter Size	Subset Size (pixel)	VSG (mm)
Plane-Strain Notch	DP1180	RD, DD, TD	0.016	3	11	31	~1.0
	DDQ	RD, DD, TD	0.016	6	15	31	~2.0
NT20 Notch	DP1180	RD, DD, TD	0.019	3	9	27	~1.0
	DDQ	RD, DD, TD	0.019	6	15	27	~2.0

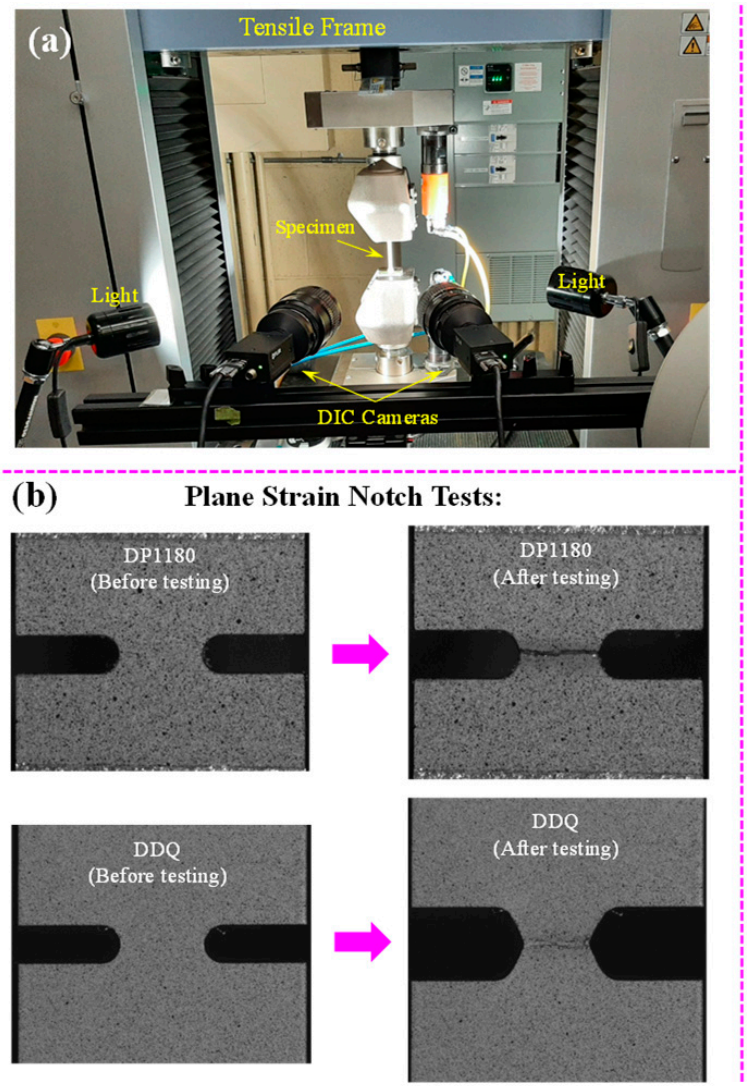

Figure 3. (**a**) Universal tensile frame and DIC setup, and (**b**) plane strain notch, and (**c**) NT20 notch specimens after and before fracture.

3. Pressure-Independent Anisotropic Plasticity under Associated Flow Rule

This section reviews several notable deviatoric yield criteria available in the literature and discusses the influence of the yield functions calibration on the plane strain regions. Generally, the parameters of anisotropic yield criteria are determined from experimental data. Conventional calibration of anisotropic yield functions has been primarily focused on utilizing only uniaxial and equal biaxial tension tests [11,25–28]; see Figure 4 for the locations of various stress states on a yield *locus*. Recent studies recognized the importance of the shear state in forming operations and employed results of shear tests as supplementary data points for calibration of advanced yield criteria [22,29,30]. Despite the importance of the plane strain condition, this state of deformation is often neglected in yield surface calibration and it is left to the phenomenological yield criterion to predict the magnitude of the principal yield stresses, as well as the stress state (or the ratio of principal stresses) in which plane strain deformation occurs. Before describing anisotropic yield functions in detail, it is beneficial to briefly review the generalized plane strain constraints of Butcher and Abedini [9] and experimental evidence supporting these constraints.

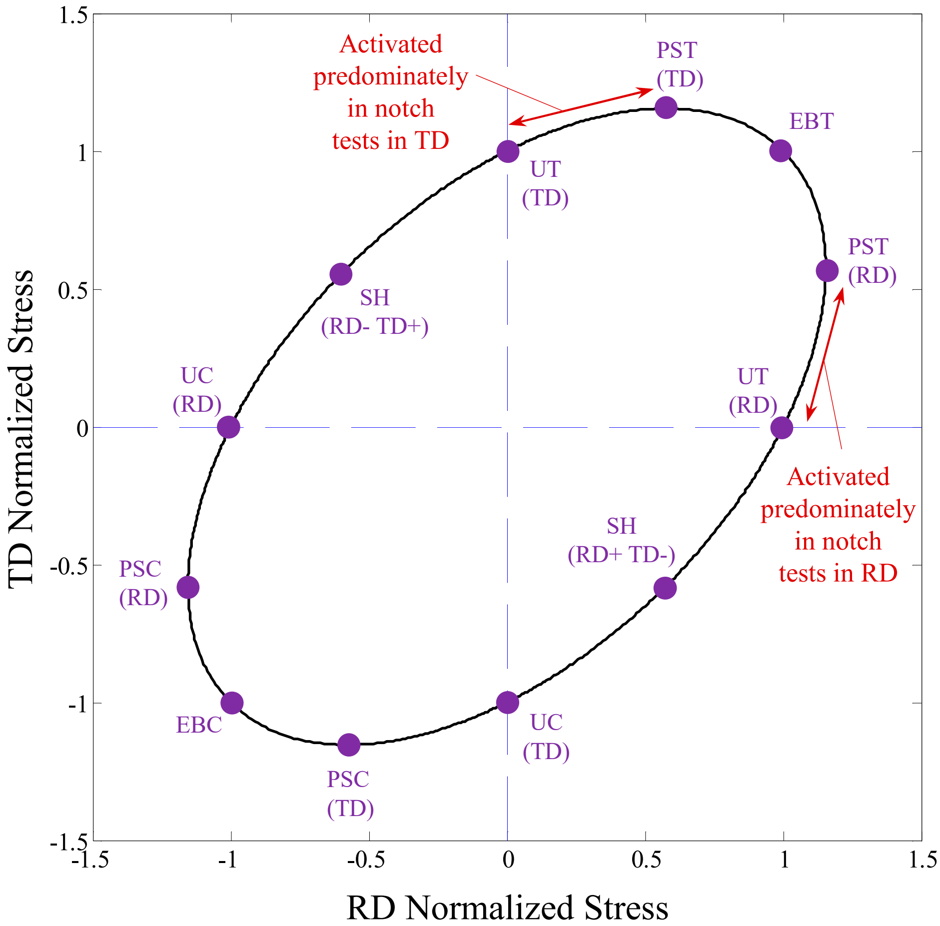

Figure 4. Schematic of a yield *locus* displaying different stress states represented in the RD-TD plane. The following abbreviations were used: UT = uniaxial tension, UC = uniaxial compression, PST = plane strain tension, PSC = plane strain compression, EBT = equal biaxial tension, EBC = equal biaxial compression, SH = shear.

3.1. Plane Strain Constraints

The importance of enforcing a new constraint on yield function calibration was first discussed by Abedini et al. [30] where it was established that a non-zero hydrostatic stress may develop if a calibration constraint is not enforced in the shear zone of anisotropic yield functions (associated flow) or plastic potentials (non-associated flow). Later, Butcher and Abedini [9] showed that the shear constraint is one case of a broader set of physically necessary constraints in "generalized plane strain conditions" for pressure-insensitive materials. This generalized state includes shear and plane strain loadings that possess a principal strain with magnitude of zero for BCC and FCC materials. HCP alloys, such as magnesium, were reported to not follow the plane strain constraints due to their complex deformation mechanisms involving twinning, which is sensitive to the hydrostatic stress.

It was discussed by Butcher and Abedini [9] that under associated anisotropic plasticity, the principal stress ratio at the plane strain extrema of deviatoric yield functions is fixed at $\frac{\sigma_2}{\sigma_1} = 0.5$ corresponding to a vanishing intermediate deviatoric stress ($s_2 = 0$). A non-zero deviatoric stress is required to produce a plastic strain increment, and vice versa, in deviatoric plasticity. In terms of deviatoric invariants, a vanishing deviatoric principal stress also corresponds to a vanishing J_3 which is commonly employed in fracture characterization to identify plane strain states [31,32]. Unfortunately, there is a misconception throughout the literature that $\frac{\sigma_2}{\sigma_1} = 0.5$ only applies to von Mises plasticity. Phenomenological yield functions obtained by applying a linear transformation upon the deviatoric stress were formulated, based upon isotropic yield functions, which remain convex under the transformation. However, the influence of the transformation upon the normal directions is not constrained. Figure 5 demonstrates that enforcing the constraint of $\frac{\sigma_2}{\sigma_1} = 0.5$ for the plane strain point results in $s_2 = 0$, while the conventional calibration does not satisfy this requirement. Applying a stress state in which $s_2 = 0$ can produce a non-zero plastic strain increment is admissible in pressure-dependent plasticity but not deviatoric pressure-independent plasticity. It is further noted that these plane strain conditions are always satisfied in the Barlat family of deviatoric yield functions in the specific case of simple shear with major principal direction at 45° to the rolling direction by virtue of how the linear transformations are applied. For simple shear at any other angle, the plane strain constraints are not automatically satisfied and will produce thinning, despite it being excluded from the applied deformation gradient.

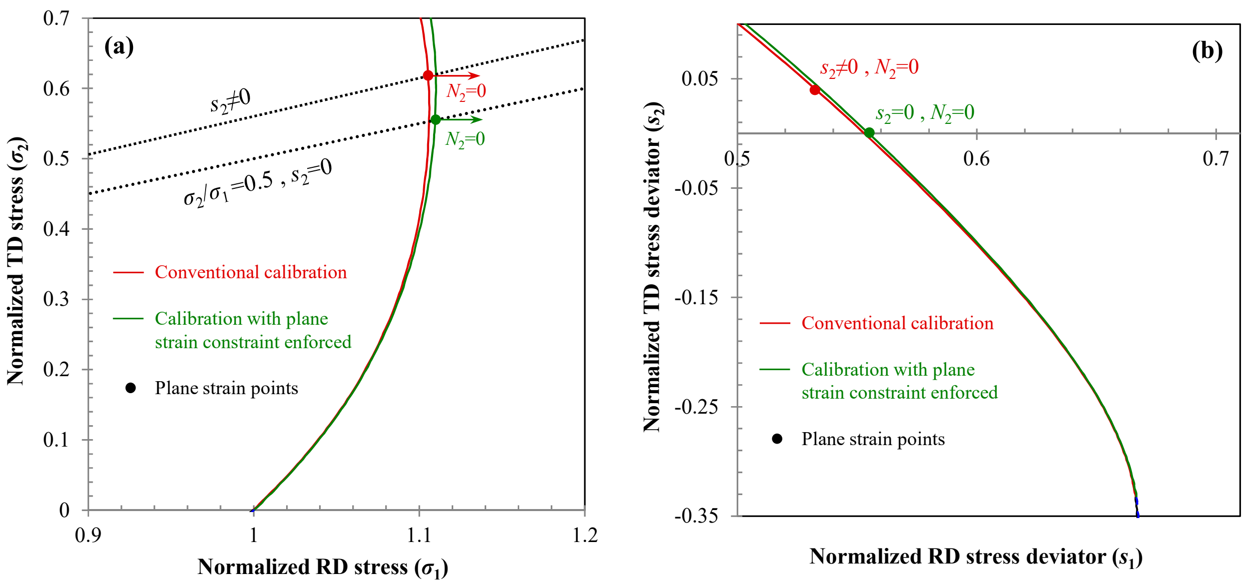

Figure 5. Yield *loci* of DP1180 calibrated using conventional calibration and a calibration with the plane strain constraint enforced plotted in (**a**) principal stress, and (**b**) principal stress deviator planes. Symbols show the plane strain points with horizontal normal vectors ($N_2 = 0$) in which only the calibration with the plane strain constraint enforced can satisfy $s_2 = 0$.

The existence of the plane strain constraint is supported by a wealth of experimental data reported in the literature. Recently, Fast-Irvine et al. [13], compiled experimental results from stress-controlled cruciform tests of various steel and aluminum alloys (labelled as Mat 1 to Mat 22 in Figure 6) and illustrated that the plane strain deformation leading to horizontal ($\beta_2 = 0°$) or vertical ($\beta_2 = 90°$) direction for the normal vector occurs when the ratio of principal stresses occurs at, or close to, the theoretical stress ratio of 1/2 ($\beta_1 = 26.6°$ or 63.4°).

It is emphasized that deviatoric plasticity is only a modeling assumption and that materials may exhibit a measure of pressure dependency, particularly for low-carbon steel grades, as recently reported by Kuwabara et al. [33]. A material with a flat yield function like a Tresca also makes it difficult to resolve the plane strain location experimentally. Nevertheless, in light of the experimental data, it appears unwise to allow the plane strain location to be completely unconstrained to fall anywhere between uniaxial and equal biaxial tension. Adopting the plane strain constraint to serve as an anchor point in the yield function calibration enables the development of a deterministic methodology to analyze notched tensile tests with inverse finite-element analysis.

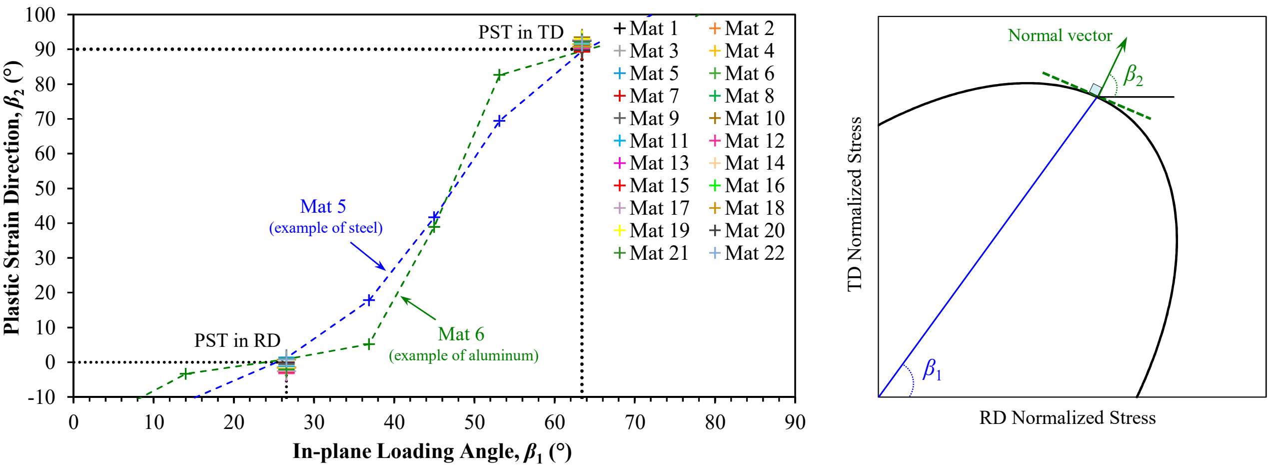

Figure 6. Experimental evidence collected by Fast-Irvine et al. [13] supporting the plane strain constraint for several body-centered cubic (BCC) and face-centered cubic (FCC) materials. For the plane strain deformation to occur, the normal vector should be either horizontal (β_2 = 0°) or vertical (β_2 = 90°) with the in-plane loading angles of β_1 = 26.6° and β_1 = 63.4° corresponding to loading along the RD and TD, respectively.

3.2. Vegter Yield Criterion

Vegter and van den Boogaard [22] proposed the so-called Vegter criterion as an anisotropic plane stress yield criterion based on interpolation by second-order Bezier curves to construct the yield surface from test data. The second-order Bezier function is developed based on two reference stress points σ_i and σ_j, and a hinge point σ_h (see Figure 7). The hinge point is the intersection of the tangents at the two reference stress points. The yield *locus* is then locally determined by:

$$\sigma_{eq}^{Vegter} = \sigma_\mathrm{i} + 2\mu(\sigma_\mathrm{h} - \sigma_\mathrm{i}) + \mu^2(\sigma_\mathrm{i} + \sigma_\mathrm{j} - 2\sigma_\mathrm{h}),\ 0 \leq \mu \leq 1 \tag{2}$$

Since the Vegter yield surface is constructed based on interpolation of yield stresses, the parameters of the model are determined directly from a set of experiments conducted for a number of directions. For each direction, experimental data from four tests are required to determine the reference points for construction of the yield *loci*: uniaxial tension, equal biaxial tension, plane strain tension, and simple shear tests. The anisotropic Vegter model has been implemented in LS-DYNA finite-element code as the material Type 136 (*MAT_CORUS_VEGTER) with seven parameters required to fully describe the second-order Bezier curve in each direction (θ): normalized uniaxial yield stress ($\frac{\sigma_\theta}{\sigma_0}$) and R-value ($R_\theta$), normalized equal biaxial yield stress ($\frac{\sigma_b}{\sigma_0}$) and equal biaxial R-value (R_b), normalized major ($\frac{\sigma_1^{PS}}{\sigma_0}$) and minor ($\frac{\sigma_2^{PS}}{\sigma_0}$) yield stress in plane strain deformation and normalized shear yield stress ($\frac{\tau_\theta}{\sigma_0}$).

To adhere to the plane strain constraints described in Section 3.1, the following relation should hold between the major and minor yield stress under plane strain deformation: ($\frac{\sigma_2^{PS}}{\sigma_0}$) = $\frac{1}{2}$ ($\frac{\sigma_1^{PS}}{\sigma_0}$). Since the major and minor yield stresses are related, for simplicity the normalized major principal stress, ($\frac{\sigma_1^{PS}}{\sigma_0}$), is referred to as the "plane strain yield stress" throughout the paper.

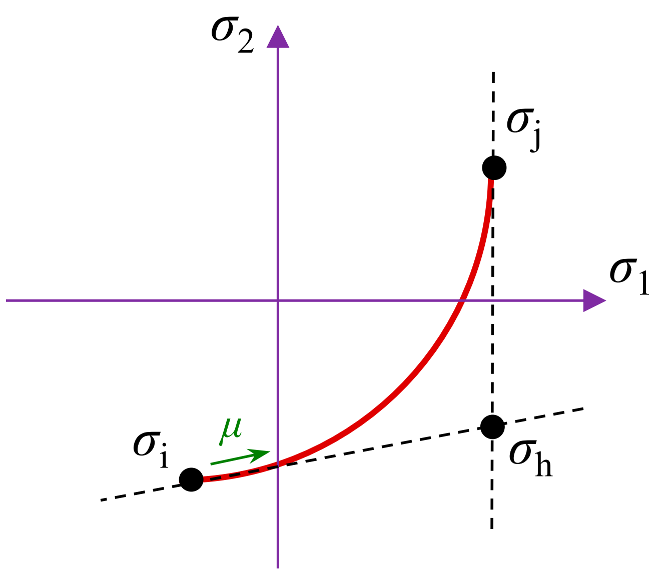

Figure 7. Bezier curve is constructed between two reference points (σ_i and σ_j) using a hinge point σ_h.

3.3. Yld2000 Yield Criterion

The well-known non-quadratic anisotropic yield criteria of Yld2000 [11] was employed in this study to act as an alternate yield surface. Detailed descriptions of the model can be found in Barlat et al. [11]. The Yld2000 yield function is defined for 2-D plane stress conditions and is written as:

$$\sigma_{eq}^{Yld2000} = \left(\frac{\phi' + \phi''}{2}\right)^{1/a} \tag{3}$$

where ϕ' and ϕ'' are given by:

$$\phi' = \left|X'_1 - X'_2\right|^a \tag{4}$$

$$\phi'' = \left|2X''_2 + X''_1\right|^a + \left|2X''_1 + X''_2\right|^a \tag{5}$$

in which $X_i{}'$ and $X_i{}''$ are the principal values of the transformed stress tensors, $\boldsymbol{X}'$ and $\boldsymbol{X}''$, and are derived by:

$$\boldsymbol{X}' = \boldsymbol{L}' : \boldsymbol{\sigma} \tag{6}$$

$$\boldsymbol{X}'' = \boldsymbol{L}'' : \boldsymbol{\sigma} \tag{7}$$

The linear stress transformation tensors are denoted by $\boldsymbol{L}'$ and $\boldsymbol{L}''$, and can be written as:

$$\boldsymbol{L}' = \begin{bmatrix} L'_{11} & L'_{12} & 0 \\ L'_{21} & L'_{22} & 0 \\ 0 & 0 & L'_{66} \end{bmatrix} \tag{8}$$

$$\boldsymbol{L}'' = \begin{bmatrix} L''_{11} & L''_{12} & 0 \\ L''_{21} & L''_{22} & 0 \\ 0 & 0 & L''_{66} \end{bmatrix} \tag{9}$$

and are defined as:

$$\begin{bmatrix} L'_{11} \\ L'_{12} \\ L'_{21} \\ L'_{22} \\ L'_{66} \end{bmatrix} = \begin{bmatrix} 2/3 & 0 & 0 \\ -1/3 & 0 & 0 \\ 0 & -1/3 & 0 \\ 0 & 2/3 & 0 \\ 0 & 0 & 1 \end{bmatrix} \begin{bmatrix} \alpha_1 \\ \alpha_2 \\ \alpha_7 \end{bmatrix} \tag{10}$$

$$\begin{bmatrix} L''_{11} \\ L''_{12} \\ L''_{21} \\ L''_{22} \\ L''_{66} \end{bmatrix} = \frac{1}{9} \begin{bmatrix} -2 & 2 & 8 & -2 & 0 \\ 1 & -4 & -4 & 4 & 0 \\ 4 & -4 & -4 & 1 & 0 \\ -2 & 8 & 2 & -2 & 0 \\ 0 & 0 & 0 & 0 & 9 \end{bmatrix} \begin{bmatrix} \alpha_3 \\ \alpha_4 \\ \alpha_5 \\ \alpha_6 \\ \alpha_8 \end{bmatrix} \tag{11}$$

where α_i are the eight anisotropy parameters of the model. In the case of isotropy, all the α_i values are set to one and the Yld2000 model is reduced to the isotropic Hosford [34] criterion.

3.4. Hardening Function

The modified Hockett-Sherby (Hockett and Sherby [35]) model of Noder and Butcher [36] was adopted to describe the hardening behavior:

$$\overline{\sigma} = B - (B - A)\left[\exp\left(-C\left(\varepsilon_{eq}^{p}\right)^{D}\right)\right] + E\sqrt{\varepsilon_{eq}^{p}} \tag{12}$$

in which A, B, C, D, and E are the coefficients of the model that were determined based on uniaxial tensile tests data up to the onset of diffuse necking. Table 3 lists the coefficients of the model and Figure 8 compares the stress-strain curves derived from the modified Hockett-Sherby model *versus* experiments in which a good agreement is evident for both materials in different directions.

Table 3. Coefficients of the hardening model determined from a uniaxial tensile test data. The inverse finite-element analysis was limited to local strains that were below the uniform elongation. The uniform elongation was enforced in the calibration process via the Considère criterion.

Materials	Modified Hockett-Sherby Model					Experiment
	A(MPa)	*B* (MPa)	*C*	*D*	*E* (MPa)	Uniform Elongation Strain
DP1180-RD	704.51	1104.65	91.91	0.88	689.05	0.071 ± 0.002
DP1180-DD	726.89	1127.60	75.11	0.87	598.47	0.066 ± 0.002
DP1180-TD	723.51	1157.59	89.18	0.88	594.46	0.065 ± 0.004
DDQ-RD	123.39	176.58	34.98	1.27	356.91	0.294 ± 0.001
DDQ-DD	136.43	191.04	55.83	1.43	354.49	0.272 ± 0.001
DDQ-TD	133.43	175.69	79.05	1.65	356.43	0.293 ± 0.004

It is necessary to emphasize that the hardening model is only considered until the local major strain in any element reaches the uniform elongation strain to avoid plastic instability and ensure the deformation is plane stress and consistent with principles of using shell elements, as described in Section 4. This termination metric follows from the Swift [37] criterion for the onset of diffuse necking in a power-law hardening material, in which the material starts to neck when the major strain reaches the n-value in both uniaxial and plane strain tension states. A critical feature of the proposed methodology is that only the measured hardening response until the UTS is used, such that extrapolations of the hardening model that may introduce bias into inverse methods are avoided. Moreover, the tensile data for each orientation is used in the analysis of the notch test to avoid the assumption of isotropic hardening. Distortional hardening, where the hardening behavior changes with the stress state, was not considered. The yield function shape was assumed to remain constant in the relatively proportional loading conditions considered in this study. Future work will examine the inclusion of more advanced hardening models and evolution of yield surface shape. It is also noted that the prediction of the material during localization and fracture was excluded from the present study, the focus of which was on characterization of the yield function during homogeneous deformation.

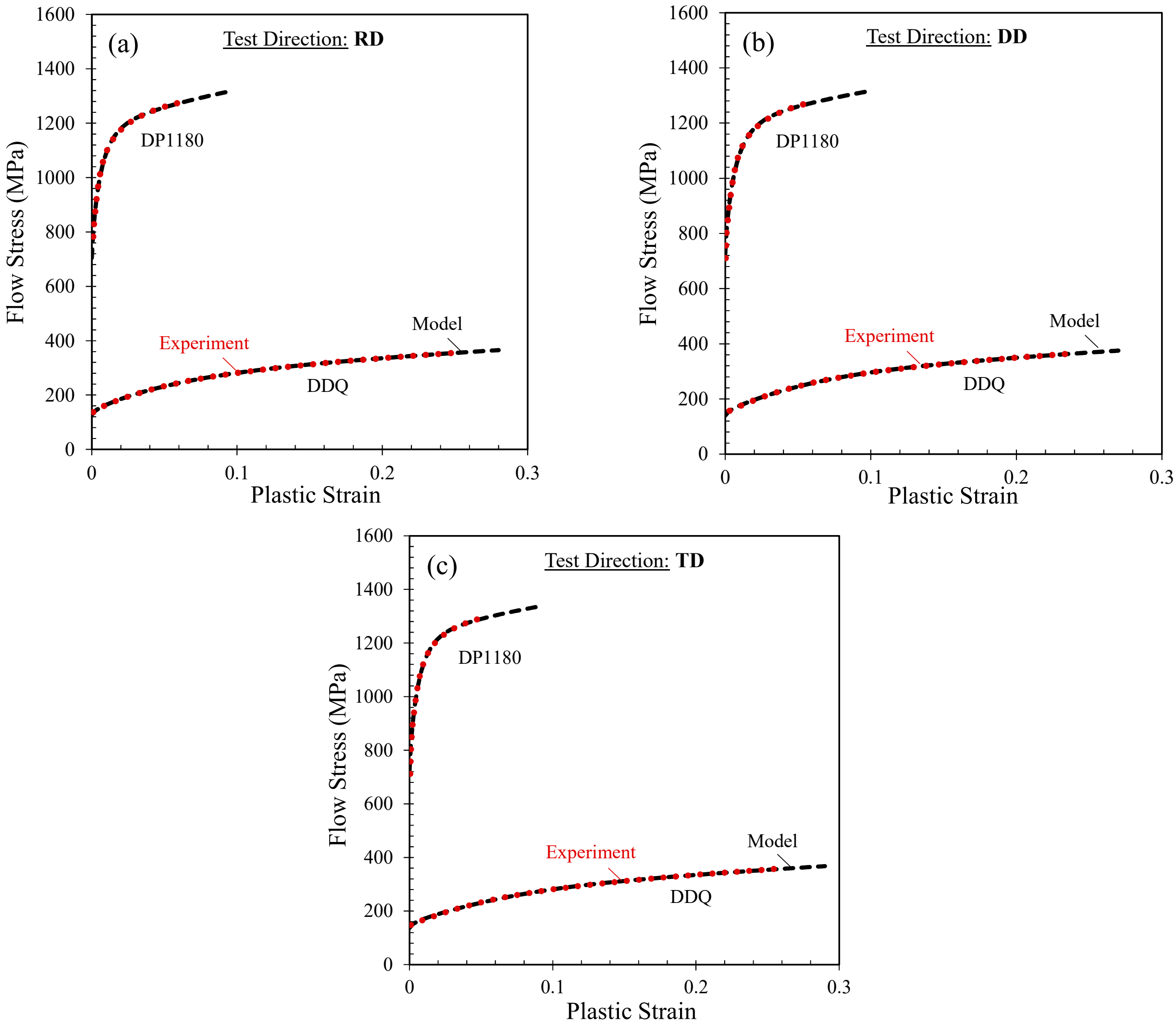

Figure 8. Hardening response of the materials in (**a**) RD, (**b**) DD, and (**c**) TD. A good agreement was obtained with the modified Hockett-Sherby model that was strictly valid until the uniform elongation strain.

3.5. Biaxial Yield Stress Estimation

Although the inverse analysis is focused on deformation between uniaxial-to-plane strain tension, it is necessary to provide the equal biaxial yield stress of the materials to the Vegter model. To provide a first-order estimate of the biaxial data, the correlations from Abspoel et al. [38] can be employed for the normalized biaxial yield stress ($\frac{\sigma_b}{\sigma_0}$):

$$\left(\frac{\sigma_b}{\sigma_0}\right) = \sigma_{un.avg}\left[\frac{\sigma_{b\_min}}{1+f_{dirac}} + \frac{\sigma_{b\_max}}{1+\frac{1}{f_{dirac}}}\right] \tag{13}$$

$$f_{dirac} = e^{[a_{dirac}(R_{avg}-\sigma_{b\_trans})]} \tag{14}$$

in which $\sigma_{un.avg}$ and R_{avg} are the in-plane averages of uniaxial yield stresses and R-values ($x_{avg} = [x_0 + 2 \times 45 + x_{90}]/4$) and the remaining parameters of Equations (13) and (14) are: $\sigma_{b\_min} = 0.97$, $\sigma_{b\_max} = 1.14$, $\sigma_{b\_trans} = 1.22$, and $a_{dirac} = 3.4$. Using the relations above, the normalized equal biaxial yield stresses for DP1180 and DDQ were estimated to be 1.024 and 1.147, respectively. The biaxial R-value, R_b, was determined using disc compression tests for both steels; nevertheless, if this data is not available, correlations for R_b are also provided by Abspoel et al. [38].

4. Inverse Finite-Element Analysis of the Plane Strain Notch Test Using Vegter Model

The non-uniform stress state across the gauge width in notch tensile tests (see Figure 4) makes it difficult to extract meaningful constitutive data directly from the test results. The applied load recorded in the experiments has contributions from all elements in the gauge area with each point subjected to a different stress state. In addition, the non-uniformity of the strain field translates to each material point experiencing a different plastic deformation or plastic work level. Finite-element analysis of the notch test can account for the local stress and strain gradients in the test and resolve the non-uniform stress/strain field in the gauge area. By constraining the material model to incorporate the measured R-value, hardening response, plane strain constraint, and restricting deformation to strain levels below the uniform elongation, the inverse finite-element analysis must only determine the magnitude of plane strain yield stress through agreement with the measured force (or nominal stress) *versus* displacement (or engineering strain) in the experiment. The Vegter model enables incorporation of experimental data in different orientations in the inverse analysis which can occur near the notch edges, as noted by Narayanan et al. [21].

The procedure for inverse finite-element analysis of plane strain notch tests is outlined as follows:

(i) Select a direction of interest (for instance, RD, DD, or TD). The input hardening curve provided to the model is associated with this direction. The analysis is repeated for all directions of interest.

1. Use available experimental data from tensile tests, i.e., normalized yield stress and R-values in different orientations, along with an initial estimate for the plane strain yield stress, and supply these values to the Vegter model. For this step, the plane strain yield stress of other directions can be assumed to be equal to the estimated plane strain yield stress of the direction of interest or they can be selected to be proportional to the normalized uniaxial yield stresses and be re-evaluated in step (iv). Shear yield stresses are of secondary importance in the current notch analysis but should be supplied to the model if the experimental data is available. In the absence of experimental results, a reasonable guess, such as the yield stress of an isotropic von Mises material (with normalized shear yield stress of 0.577), can be used.

(iii) Iteratively update the plane strain yield stress until a good agreement between experimental and numerical global response of the material is reached. Increasing the plane strain yield stress leads to a stronger uniaxial-to-plane strain response and, consequently, a higher load is resolved and vice versa.

(iv) Once all directions of interest are evaluated, re-run the model with the resolved plane strain yield stresses for all directions, and, if necessary, make any final adjustments to the plane strain yield stresses.

The outcome of the analysis will be the plane strain yield stresses for different directions. It should be noted that the calibrated Vegter model can act as a "master yield surface" incorporating different stress states and orientations. Nevertheless, due to the widespread industrial use of the Barlat-family of yield criteria, the results of the inverse analysis using the Vegter model is utilized in Section 5.4 to calibrate the Yld2000 model.

This deterministic approach is only made possible due to the enforcement of the plane strain constraint to keep the plane strain stress state fixed. Without the plane strain constraint enforced, results of the inverse analysis would vary with the choice of anisotropic yield function, since the stress state in plane strain deformation is taken as unknown. Of particular relevance is the inverse analysis of notched tests by Suh et al. [39] using the Hill79 [40] and Yld91 [10] models. The inverse analysis led to a different constitutive response in plane strain for each yield criterion since the plane strain location on the yield surfaces did not remain constant. Consequently, the local arc of each yield *locus* and plane strain yield strength identified by Suh et al. [39] varied for each model to satisfy the global force response. These pitfalls are avoided by exploiting the plane strain constraint to identify the magnitude of the plane strain yield strength and the arc from uniaxial-to-plane strain tension. The NT20 notch tests can then be used to identify the accuracy of the calibrated arc for both materials in Section 5.3.

Finite Element Model Parameters

Finite element models of the two notched specimens were created and analyzed with the commercial finite-element code, LS-DYNA, using explicit time integration. Due to symmetry, only half of the notch samples were modeled, as depicted in Figure 9. The boundary conditions consisted of imposing a zero displacement in the direction perpendicular to the axes of symmetry. Velocity-controlled boundary conditions (0.005 mm/s cross-head velocity in the plane strain notch test and 0.030 mm/s cross-head velocity for the NT20 notch specimen) were applied to the upper nodes to resemble the moving grip, while the displacement of lower nodes was restricted to resemble the clamped condition of the fixed grip.

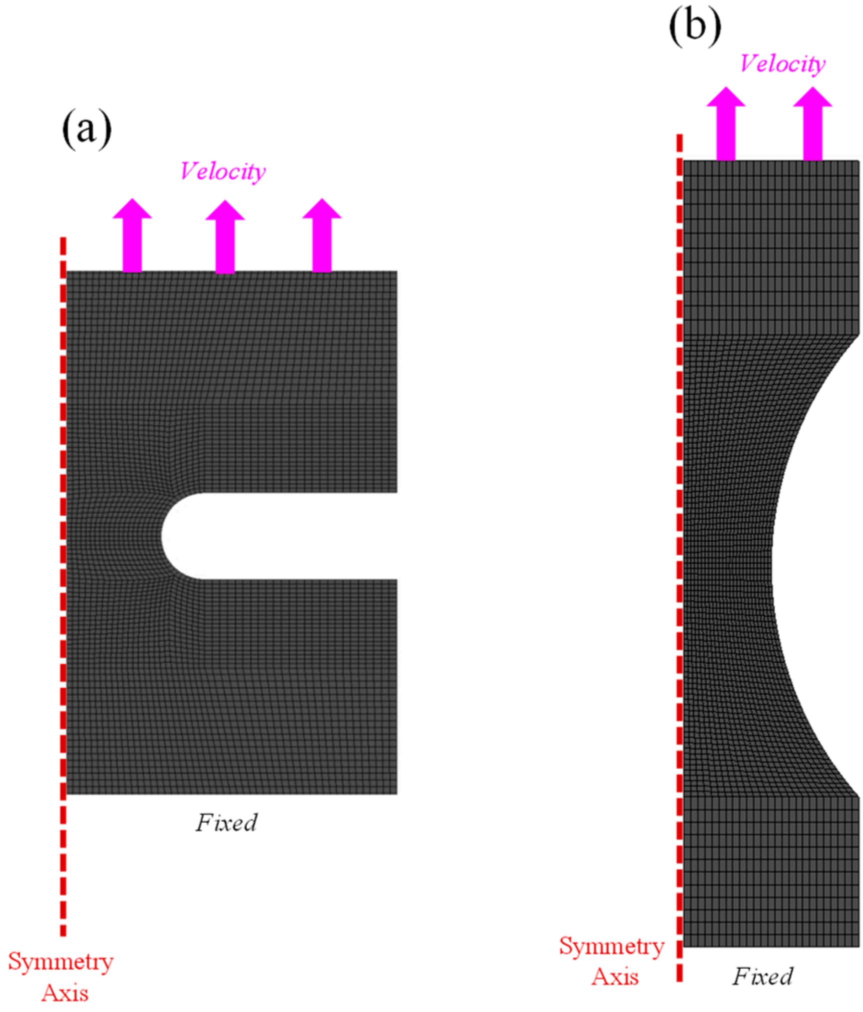

Figure 9. Discretized models of (**a**) plane strain notch and (**b**) NT20 notch specimens considering symmetry with the symmetry axes depicted.

An average shell element size of ~0.20 mm was used in the gauge area. A mesh sensitivity study demonstrated that the global response before the onset of localization remained unaffected when smaller element sizes were employed. Recall that the inverse analysis is terminated when the deformation level of an element reaches the uniform elongation strain. The results of the mesh sensitivity analysis are detailed in Appendix A. Shell element Type 16 in LS-DYNA (fully-integrated shell elements) was employed for the simulations. The plane strain and NT20 notch models included 4953 and 2860 nodes, respectively. The total number of elements were 4822 and 2725 for the plane strain and NT20 notch specimens, respectively.

5. Results and Discussion

5.1. Global Response of Plane Strain Notch Specimen

The inverse analysis consisted of varying the plane strain yield strength while keeping the other critical plasticity properties (like uniaxial yield stress, R-values, hardening curve, etc.) fixed with an objective to achieve good correlation between the global response of the model and experiments. Figure 10a shows the engineering stress-strain response of notch tensile tests for DP1180 in the RD. The far-field engineering strain, $\Delta L/L_0$, was calculated with a L_0 = 16.0 mm gauge length (see Figure 2a). The engineering stress was the measured load divided by the initial cross-sectional area, F/A_0. The results are shown up to the level of engineering strain at which the edge element reached the uniform elongation strain from the uniaxial tension tests. As shown in Figure 10b, increasing the plane strain yield stress resulted in a higher extremum of the yield *locus* in the uniaxial-to-plane strain region and, consequently, a larger engineering stress was predicted (Figure 10a). A plane strain yield stress of ~1.10 provided good correlation between experimental and finite-element model engineering stress-strain results for DP1180 in the RD.

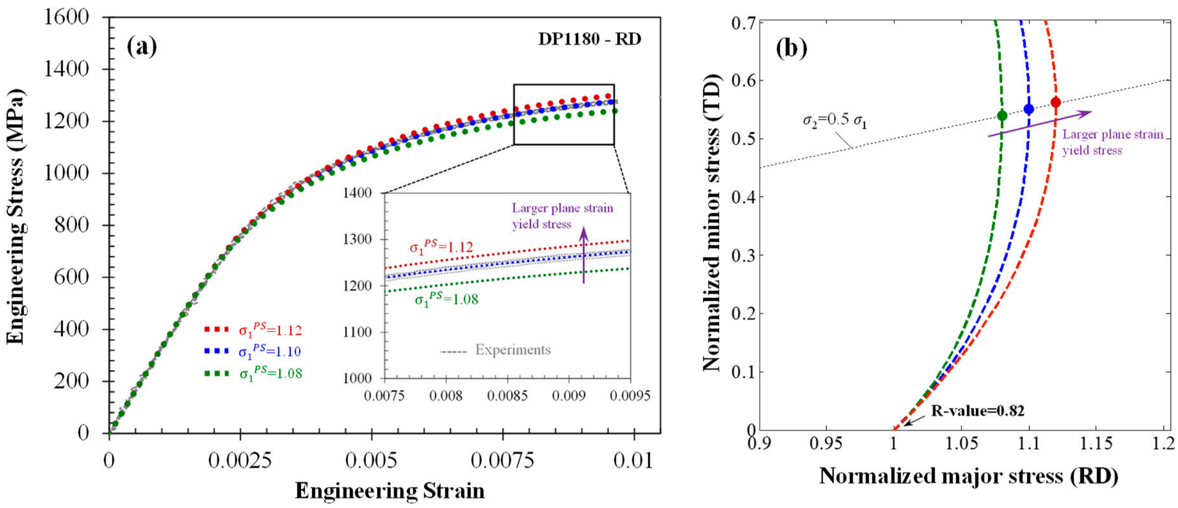

Figure 10. (**a**) Engineering stress-strain response of the DP1180 in the RD, (**b**) yield *loci* in the tensile region demonstrated that increasing the plane strain yield stress had a direct impact on the engineering stress-strain behavior of the material.

The same procedure was followed for the tests conducted in other directions for the DP1180 (DD and TD), as well as the DDQ in the RD, DD, and TD, with the results of the inverse analysis for all directions depicted in Figures 11 and 12, for DP1180 and DDQ, respectively. For comparison, the yield *locus* of the isotropic von Mises criterion was also plotted along with that of the Vegter at each direction. To quantify accuracy of the predictions, the mean absolute error (MAE) was calculated using the following relation:

$$Error = \frac{1}{n}\sum_{i=1}^{n}\left|x_i^{predicted} - x_i^{measured}\right| \quad (15)$$

in which x is the quantity of interest (engineering stress in this case), and n is the number of data points used to calculate the error. The ranges of engineering strain plotted in Figures 11 and 12 were divided into 50 equally spaced points (n = 50), and the corresponding *Error* values for engineering stress were calculated and reported in Table 4. It was apparent that the *Error* was below 5.0 MPa for the different directions of the two materials.

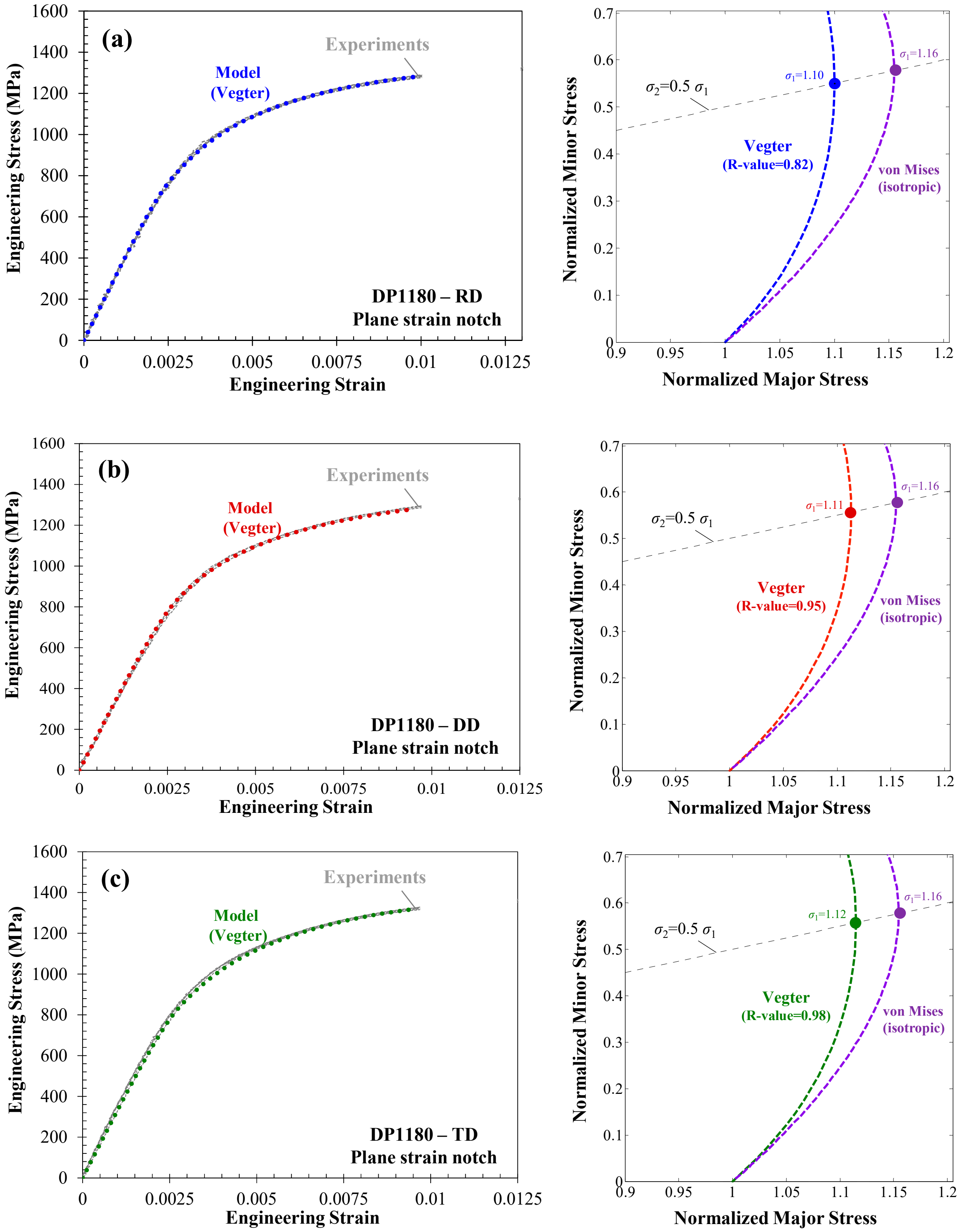

Figure 11. Engineering stress-strain response of plane strain notch tests extracted from models and experiments along with the yield *loci* for DP1180 in (**a**) RD, (**b**) DD, and (**c**) TD. A gauge length of 16 mm was used to calculate far-field strains in the models and experiments.

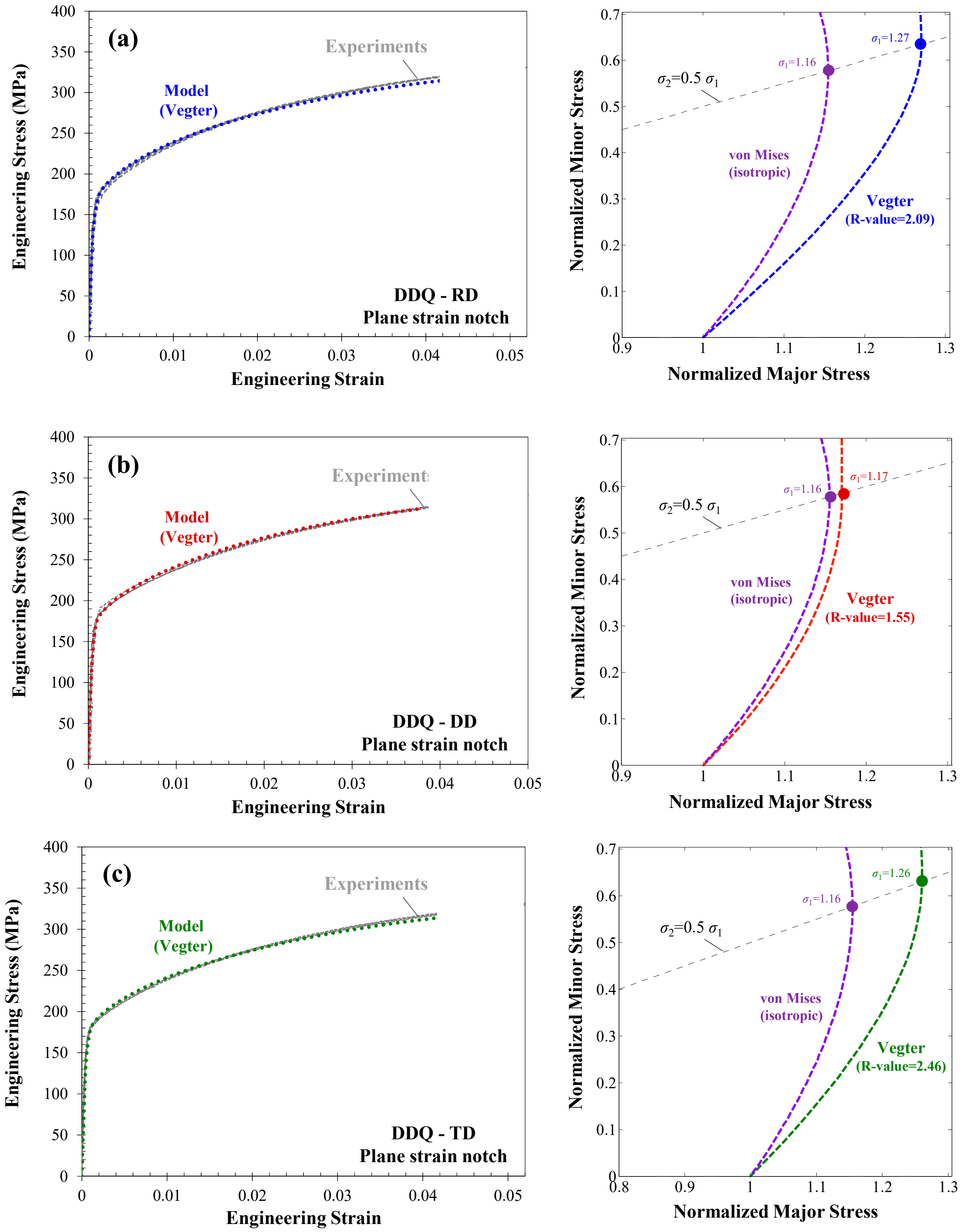

Figure 12. Engineering stress-strain response of plane strain notch tests extracted from models and experiments along with the yield *loci* for DDQ in (**a**) RD, (**b**) DD, and (**c**) TD. A gauge length of 16 mm was used to calculate far-field strains in the models and experiments.

Table 4. *Error* (Equation (15)) in resolving measured engineering stress, major strain, and minor strain for the plane strain notch tests.

Material-Direction	*Error* (Eng. Stress) [MPa]	*Error* (Major Strain)	*Error* (Minor Strain)
DP1180-RD	4.01 ± 1.28	0.0006 ± 0.0003	0.0007 ± 0.0006
DP1180-DD	4.17 ± 1.54	0.0015 ± 0.0009	0.0012 ± 0.0004
DP1180-TD	4.95 ± 1.95	0.0008 ± 0.0001	0.0006 ± 0.0002
DDQ-RD	2.49 ± 0.31	0.0026 ± 0.0003	0.0005 ± 0.0001
DDQ-DD	2.02 ± 0.57	0.0008 ± 0.0003	0.0007 ± 0.0001
DDQ-TD	2.38 ± 0.42	0.0016 ± 0.0005	0.0005 ± 0.0002

The identified values of the normalized plane strain yield strength are presented in Table 5. The inverse analysis showed that for DP1180 with R-values of below unity, the normalized plane strain yield stress was in the range of 1.10 to 1.14. In contrast, for DDQ steel featuring significantly larger R-values, the plane strain yield strength was notably stronger, with values ranging from 1.22 to 1.27, depending on the orientation. It appeared that the plane strain yield strength and tensile R-values were directly related (increasing the R-value leads to a larger plane strain yield stress) which was in general agreement with the observations of Abspoel et al. [38] and Narayanan et al. [21]. However, the DDQ in TD with the large R-value of 2.46 was a counter example for this trend, where the plane strain yield stress ($\frac{\sigma_1^{PS}}{\sigma_0}$ = 1.25) was lower than that of the RD ($\frac{\sigma_1^{PS}}{\sigma_0}$ = 1.27) with the R-value of 2.09.

Table 5. Normalized plane strain yield strengths in different orientations derived from the inverse analysis of notch tension tests.

Material-Direction	Normalized Yield Strength	Normalized Yield Strength w.r.t RD
DP1180-RD	1.10	1.10
DP1180-DD	1.11	1.12
DP1180-TD	1.12	1.14
DDQ-RD	1.27	1.27
DDQ-DD	1.17	1.22
DDQ-TD	1.26	1.25

5.2. Local Response of the Plane Strain Notch Specimen

For simplicity, the developed inverse analysis is primarily focused on the global behavior of the materials in terms of load-displacement or nominal stress-strain response. Nevertheless, the methodology could be extended to incorporate local response of the materials in regard to local strains measured by means of the DIC. This extension could potentially assist with improving the local predictions at a cost of more complexity in optimization of the parameters of anisotropic plasticity models. The present analysis was based upon associated plasticity, so a significant difference between the global stress response and local strains might be attributed to non-associated plasticity effects. Future work is required to consider non-associated plasticity, as it increases the degrees of freedom in the calibration procedure.

An investigation into local DIC strains measured with a point inspector at the center of the gauge region of the plane strain notch specimen showed that the anisotropic Vegter model was able to capture the local behavior of the two materials with good accuracy. As evident from Figures 13 and 14, that illustrate the strain paths in terms of major (ε_1) versus minor (ε_2) strains, the predicted strain paths were in excellent agreement with experiments, except for the DDQ tests in the RD and TD where the predicted strain paths were slightly tilted toward the drawing (left) side compared to the experiments. It was also apparent that the strain state at the center of the specimen was close to plane strain tension with minor strains notably smaller than the major strain $\varepsilon_2/\varepsilon_1 \approx 0$. The magnitude of the minor strain remained lower than 0.004 for both materials. The MAE metric for quantifying the error between the model predictions and measured values (Equation (15)) were also adopted for the local values and the associated errors are reported in Table 4.

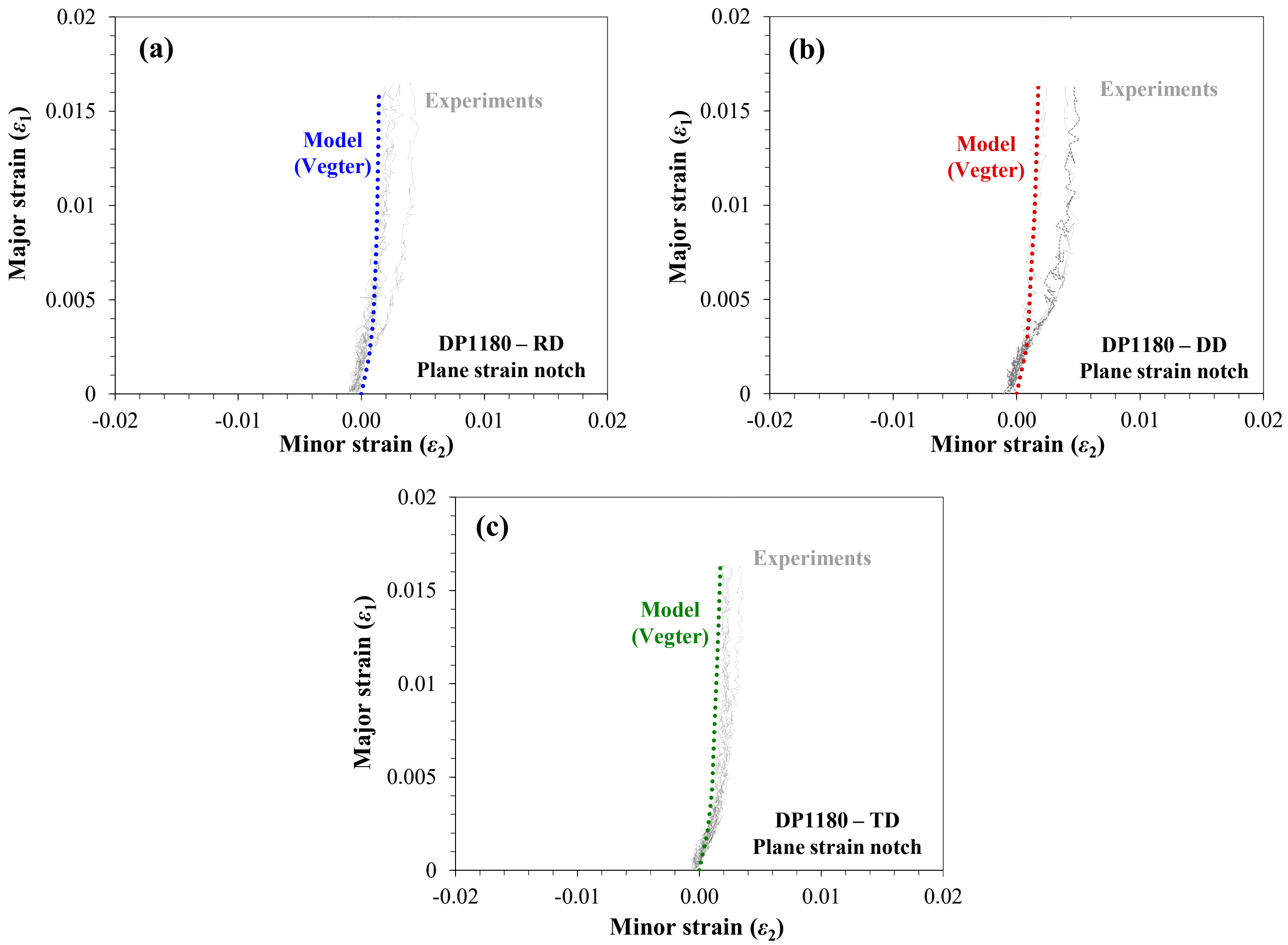

Figure 13. Measured DIC strain paths at the center of the plane strain notch tests compared to model predictions for DP1180 in (**a**) RD, (**b**) DD, and (**c**) TD.

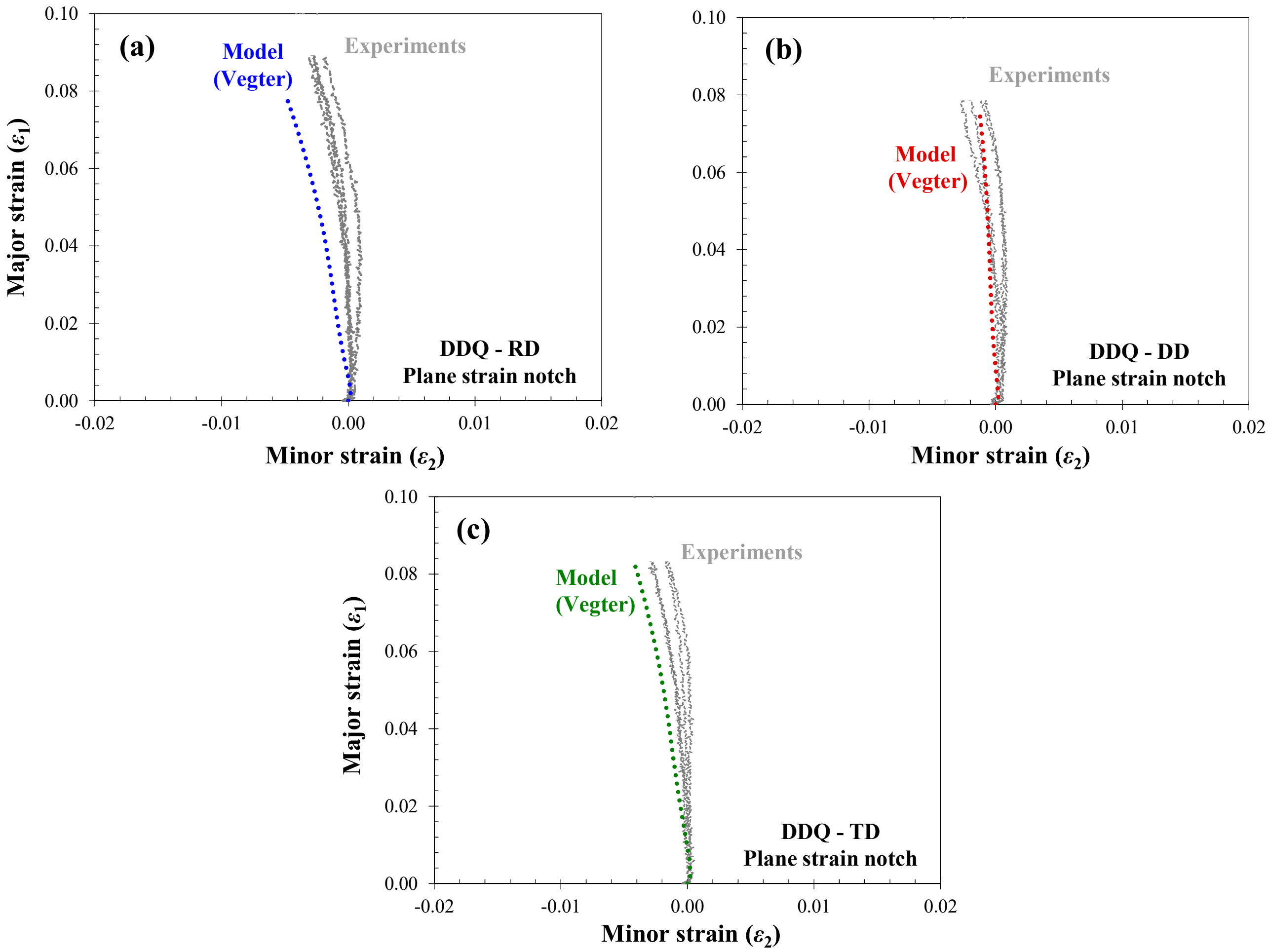

Figure 14. Measured DIC strain paths at the center of the plane strain notch tests compared to model predictions for DDQ in (**a**) RD, (**b**) DD, and (**c**) TD.

5.3. Evaluation of the Yield Functions Using the NT20 Notch Test

To evaluate the predictive capabilities of the calibrated Vegter model, tensile tests with the NT20 notch specimen were conducted in the three directions (RD, DD, TD) for the two materials. The selected geometry activated stress states between uniaxial and plane strain tension and served as an assessment test for the developed methodology. Figures 15 and 16 compare the engineering stress-strain and local strains at the center of the specimen of the models *versus* experiments for DP1180 and DDQ, respectively, and Table 6 presents the prediction errors determined with Equation (15). For the DP1180, the predicted responses compared favorably with the experiments, indicating that the calibrated Vegter model was robust in reproducing the response of the material in uniaxial-to-plane strain region. For DDQ, the engineering stress-strain responses from the model were marginally underestimated, while the predicted strain paths were shifted toward the draw side. Nevertheless, the overall performance of the model was reasonable for DDQ.

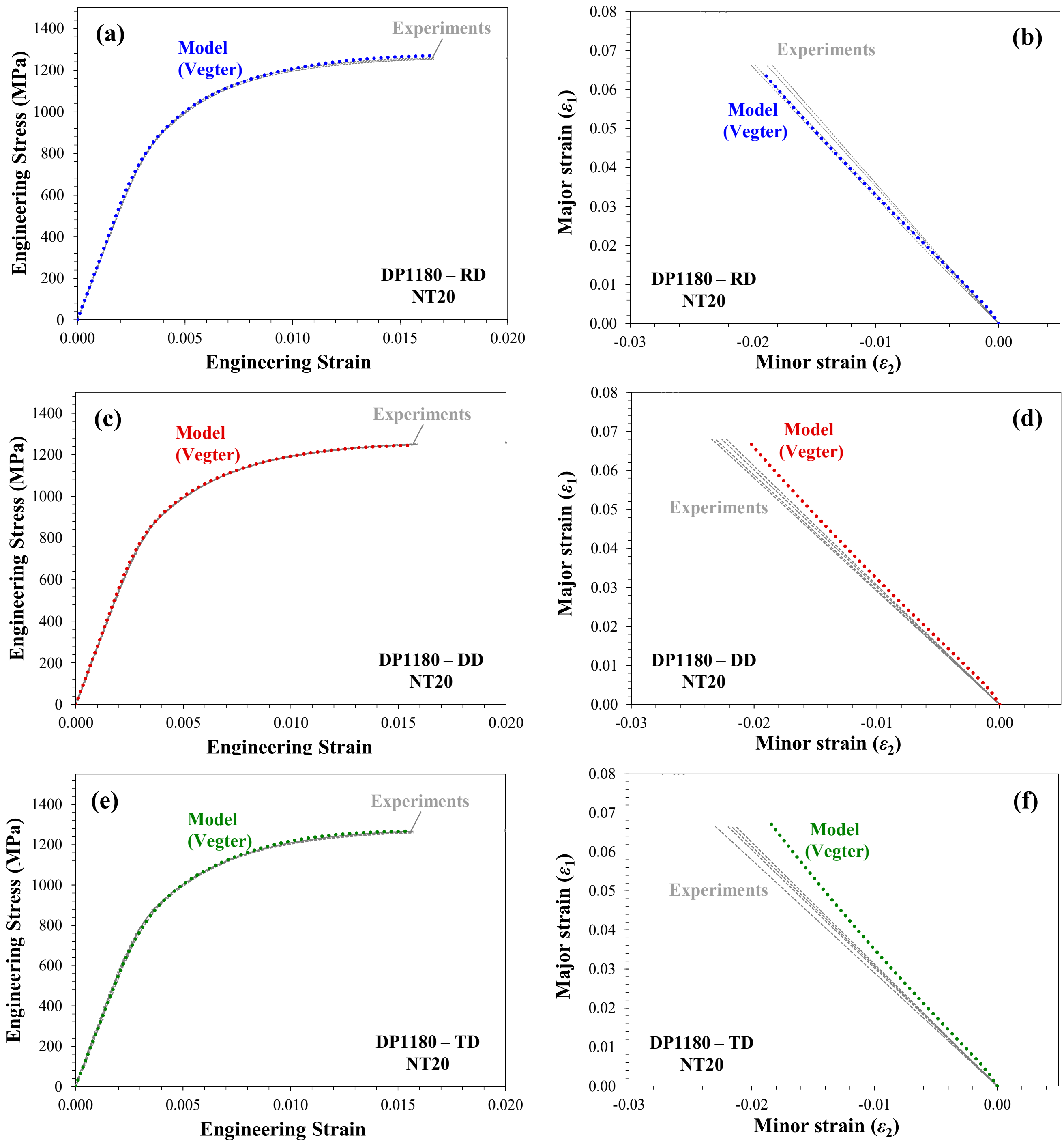

Figure 15. Engineering stress-strain response and local strain paths extracted from NT20 models and experiments for DP1180 in (**a**,**b**) RD, (**c**,**d**) DD, and (**e**,**f**) TD. A gauge length of 35 mm was used to calculate far-field strains in the models and experiments and the local strain paths were extracted from the center of the specimen.

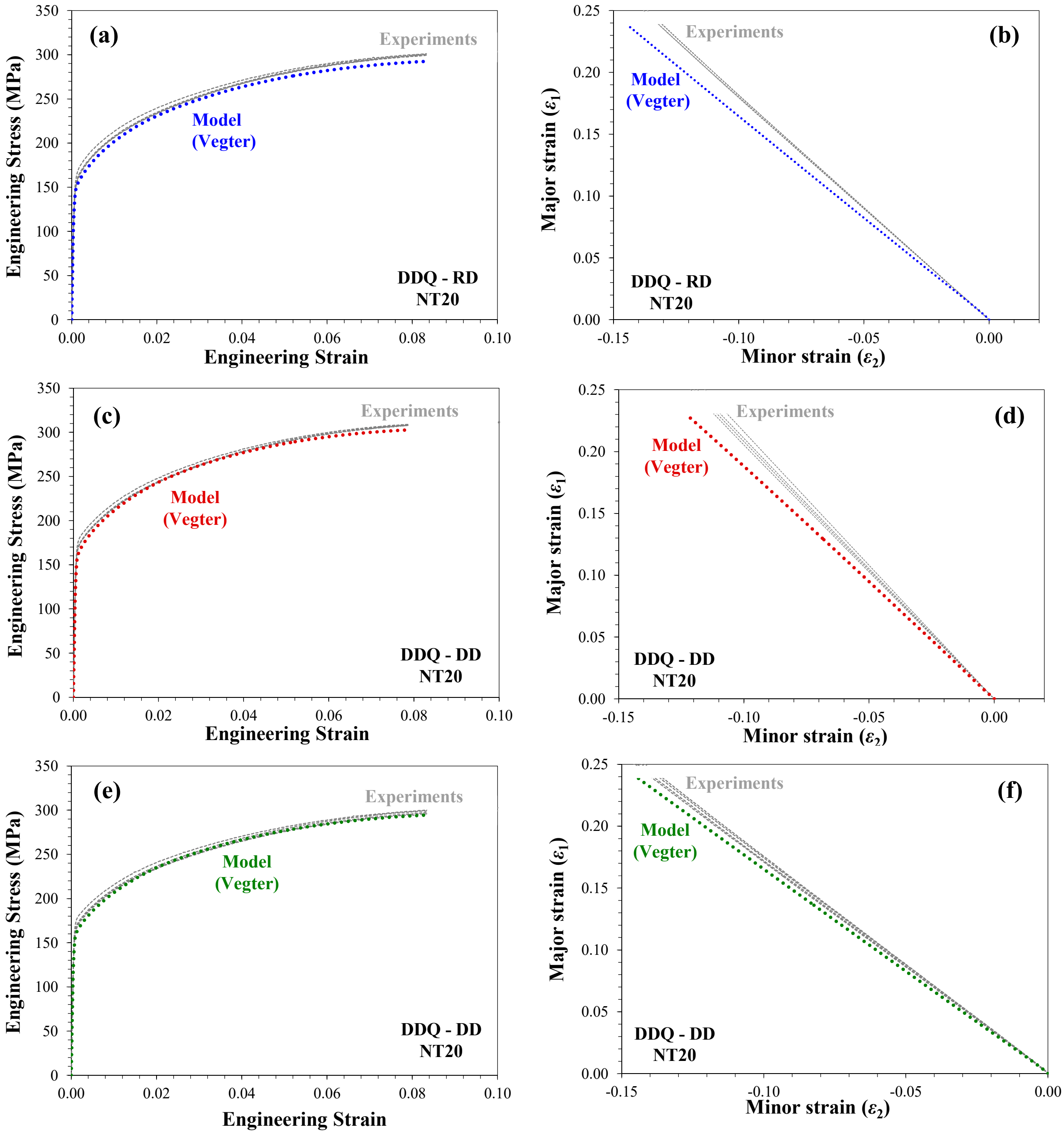

Figure 16. Engineering stress-strain response and local strain paths extracted from NT20 models and experiments for DDQ in (**a**,**b**) RD, (**c**,**d**) DD, and (**e**,**f**) TD. A gauge length of 35 mm was used to calculate far-field strains in the models and experiments and the local strain paths were extracted from the center of the specimen.

Table 6. *Error* (Equation (15)) in resolving measured engineering stress, major strain, and minor strain for the NT20 notch tests.

Material-Direction	*Error* (Eng. Stress) [MPa]	*Error* (Major Strain)	*Error* (Minor Strain)
DP1180-RD	7.22 ± 3.35	0.0053 ± 0.0007	0.0019 ± 0.0005
DP1180-DD	4.06 ± 2.10	0.0063 ± 0.0004	0.0053 ± 0.0004
DP1180-TD	6.23 ± 2.05	0.0071 ± 0.0005	0.0073 ± 0.0004
DDQ-RD	5.83 ± 1.92	0.0165 ± 0.0017	0.0158 ± 0.0016
DDQ-DD	3.36 ± 1.50	0.0161 ± 0.0014	0.0127 ± 0.0007
DDQ-TD	2.87 ± 1.94	0.0103 ± 0.0014	0.0097 ± 0.0013

This analysis verified the predictions of the Vegter model in the uniaxial-to-plane strain region. The model in its current form could be used for formability and fracture applications. Alternatively, if desired, the resolved plane strain yield strength could be used along with the standard characterization data of plasticity to calibrate other advanced yield criteria, such as the Yld2000 model [11], as described in Section 5.4.

5.4. Calibration of an Alternate Yield Surface

The interpolative nature of the Vegter model enabled a straightforward calibration process for the notch tension tests. The Vegter model enabled specific regions of the yield surface to be adjusted. Although alternate models, such as the Yld2000 yield criterion of Barlat et al. [11], could be used instead of Vegter, it is difficult to ensure that only a specific region of the yield surface changes while keeping the remainder regions unchanged. However, the Vegter model is not widely used by industry, in which closed-form yield functions are preferred. Therefore, the calibrated Vegter model could, instead, be used to calibrate the Yld2000 model once the inverse analysis was completed.

For each material, the following inputs were used to calibrate the Yld2000 yield function:

Stress anisotropy: Uniaxial tensile yield stress in different orientations with respect to the RD (0°, 15°, 30°, 45°, 60°, 75°, and 90° for DP1180 and 0°, 22.5°, 45°, 67.5°, and 90° for DDQ), shear stress in three directions (0°, 22.5°, 45°), and plane strain stress in three directions (0°, 45°, 90°) obtained from the inverse finite-element analysis. In addition, yield stresses of five intermediate points equally spaced between uniaxial and plane strain tension for the three directions (0°, 45°, 90°) were derived from the Vegter model to guide the calibration of the Yld2000 model to reproduce the determined uniaxial to plane strain arcs. The estimations from Abspoel et al. [38] for equal biaxial yield stress (Section 3.5) were also used in the calibration of the yield function.

Plastic anisotropy: Uniaxial tensile R-values in different directions (0°, 15°, 30°, 45°, 60°, 75°, and 90° for DP1180 and 0°, 22.5°, 45°, 67.5°, 90° for DDQ), equal biaxial R-value, and the generalized plane strain constraint of Butcher and Abedini [9].

Table 7 presents the coefficients of the Yld2000 model for both materials and Figures 17a and 18a display the yield loci of DP1180 and DDQ, respectively, where the data points used for calibration are illustrated with red symbols. In addition, Figures 17b and 18b depict the model predictions for normalized plane strain, shear, and tensile stresses and R-values. For comparison, the results of the Vegter criterion are also plotted. Comparing the two materials, calibration of the Yld2000 model was particularly more challenging for the DDQ that featured significantly larger R-values compared to DP1180. Nevertheless, it can be seen that for both materials the Yld2000 model exhibited good correlation with the experimental results as well as the calibrated Vegter criterion in all stress states and orientations with an exception of normalized shear stresses that were better resolved by the Vegter model. It is noted that the materials were assumed as orthotropic and tension-compression symmetric, which is in line with the orthotropic-symmetric formulations of the Yld2000 and the Vegter criteria.

Table 7. Coefficients of the Yld2000 yield criterion for DP1180 and DDQ. A yield exponent of 6.0 was utilized as suggested for BCC materials.

Coefficient	DP1180	DDQ
α_1	0.9684	1.0125
α_2	0.9864	1.0752
α_3	1.0303	0.7966
α_4	0.9855	0.8816
α_5	1.0066	0.9032
α_6	0.9582	0.8092
α_7	0.9943	0.9883
α_8	1.0158	1.0213
a	6.0	6.0

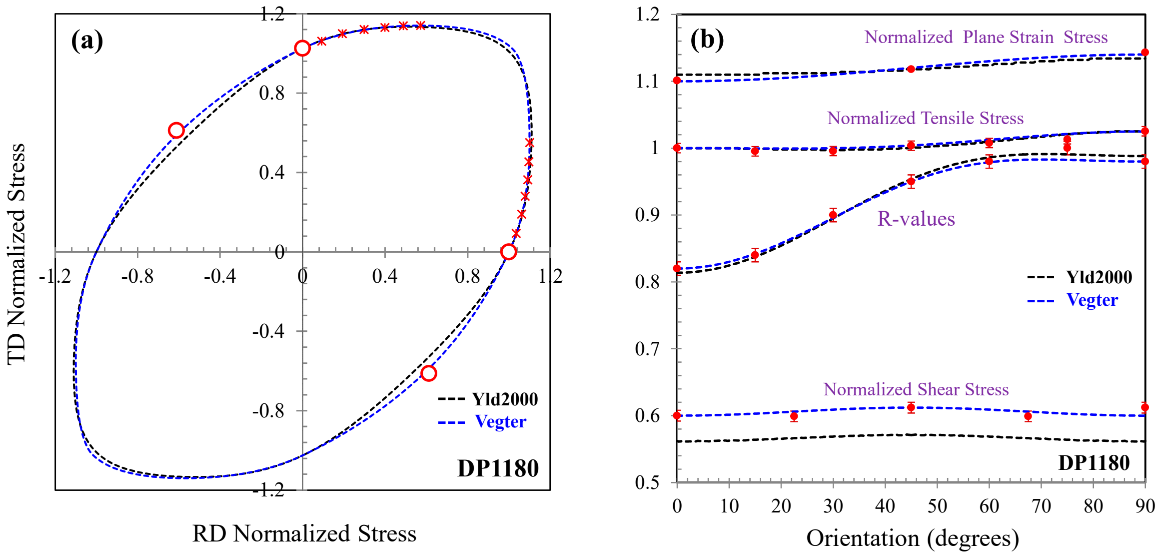

Figure 17. (**a**) The Yld2000 and Vegter yield loci and (**b**) normalized stresses and R-values predictions for DP1180. Symbols indicate the data used for calibration.

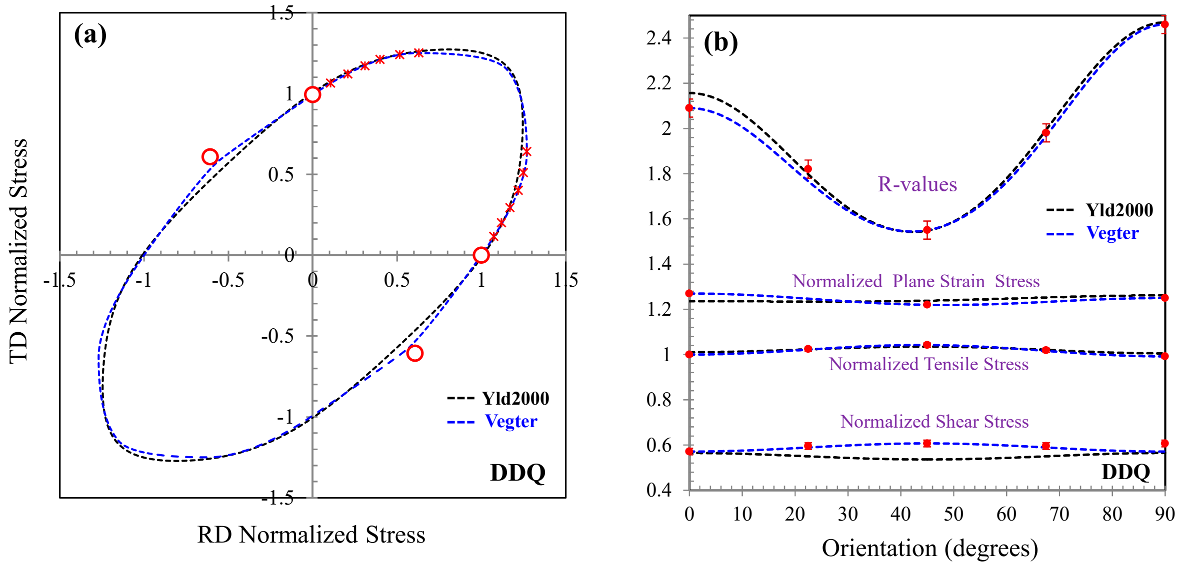

Figure 18. (**a**) The Yld2000 and Vegter yield loci and (**b**) normalized stresses and R-values predictions for DDQ. Symbols indicate the data used for calibration.

6. Conclusions

Due to the lack of reliable plane strain constitutive data, the conventional calibration of anisotropic yield functions is primarily based on using only uniaxial and biaxial tensile data, and, consequently, calibration of the plane strain region of yield surfaces is neglected. Thus, yield strength of anisotropic materials under plane strain deformation is typically *predicted* by phenomenological yield criteria and left unverified. Given the critical role of plane strain deformation in formability and fracture, the conventional calibration approach may result in an incorrect plane strain yield strength and may adversely impact forming and crashworthiness simulations. The present paper proposed a straightforward user-friendly methodology to estimate the plane strain yield strength of materials by means of inverse finite-element analysis of notch tension specimens. The methodology is based on employing the Vegter criterion, restricted with the generalized plane strain constraints of Butcher and Abedini [9], to perform in accordance with the mechanics of plane strain deformation. The following points were established by the present study:

- The inverse finite-element approach can take advantage of the non-uniformity in the stress/strain field of notch specimens to calibrate the arc of the associated yield surface from uniaxial to plane strain tension. The yield stress under plane strain deformation of the Vegter function was used as a control variable to match the global load-displacement response of the model and experiments for DP1180 and DDQ sheets.
- Although the inverse analysis was primarily focused on global response of the materials in terms of engineering stress-strain curves, it was established that the local response of the materials at the center of the gauge region was also predicted with good accuracy.
- It was demonstrated that the calibrated Vegter yield function can precisely capture local and global response of an alternate notch tensile geometry and the predictive capability of the model was verified.
- Once the plane strain regions of the materials were characterized by the proposed technique in different directions, the Yld2000 model was used as an alternate yield criterion where the model was able to describe the response of the materials in a wide range of stress states, including the plane strain regions resolved from the inverse analysis.

Author Contributions: Conceptualization, methodology, A.A. and C.B.; formal analysis, writing—original draft preparation, A.A.; investigation, validation, A.A. and A.N.; writing—review & editing, A.A., C.B. and A.N.; supervision, project administration, C.B. All authors have read and agreed to the published version of the manuscript.

Funding: This research was funded by Natural Sciences and Engineering Research Council of Canada (NSERC), Discovery Grant (grant number: RGPIN-2017-04716).

Data Availability Statement: Not applicable.

Acknowledgments: The authors would like to thank members of the Nonlinear Strain Path Project Team of the Auto/Steel Partnership (A/SP) for technical and financial support. Financial support was also provided by the Natural Sciences and Engineering Research Council of Canada (NSERC). The authors would like to acknowledge Cole Fast-Irvine and Jacqueline Noder of the University of Waterloo for their assistance with experiments and analysis.

Conflicts of Interest: The authors declare no conflict of interest.

Appendix A. Mesh Sensitivity Analysis

A mesh sensitivity analysis was carried out to investigate the effect of element size, type, formulation, and aspect ratio on the predicted global and local responses of the simulations. As discussed by Inguez-Macedo et al. [41], it is critical to take into consideration the effects of these parameters in the results of finite-element simulations. Since the methodology developed in the present study was based on the plane strain notch specimen, the mesh sensitivity analysis was performed for this geometry only. As not all element types are applicable for anisotropic materials, an isotropic von Mises material was assumed with properties of DDQ steel (thickness and hardening function) to evaluate the mesh sensitivity in the plane strain notch simulation with solid and shell elements. The DDQ material was selected for the mesh sensitivity analysis because it possesses the largest uniform elongation and thickness to better demonstrate potential mesh effects and through-thickness gradient effects between solid and shell elements.

Appendix A.1. Effect of Element Type

The effect of element type (shell versus solid) was examined using two models with an element size of 0.20 mm with the solid model including five elements through the half thickness of the sheet with an aspect ratio (*AR*) of unity, see Figure A1. Both solid and shell elements were selected to be fully integrated (Type 16 and Type 2 in LS-DYNA for shells and solids, respectively). It can be seen that, while the model with shell elements localized early and could not properly capture the post-uniform response, it was in excellent agreement with the results of the solid model before the first element at the edge reached the uniform strain (shown with a symbol in Figure A1). Recall that the proposed inverse analysis was terminated at this point.

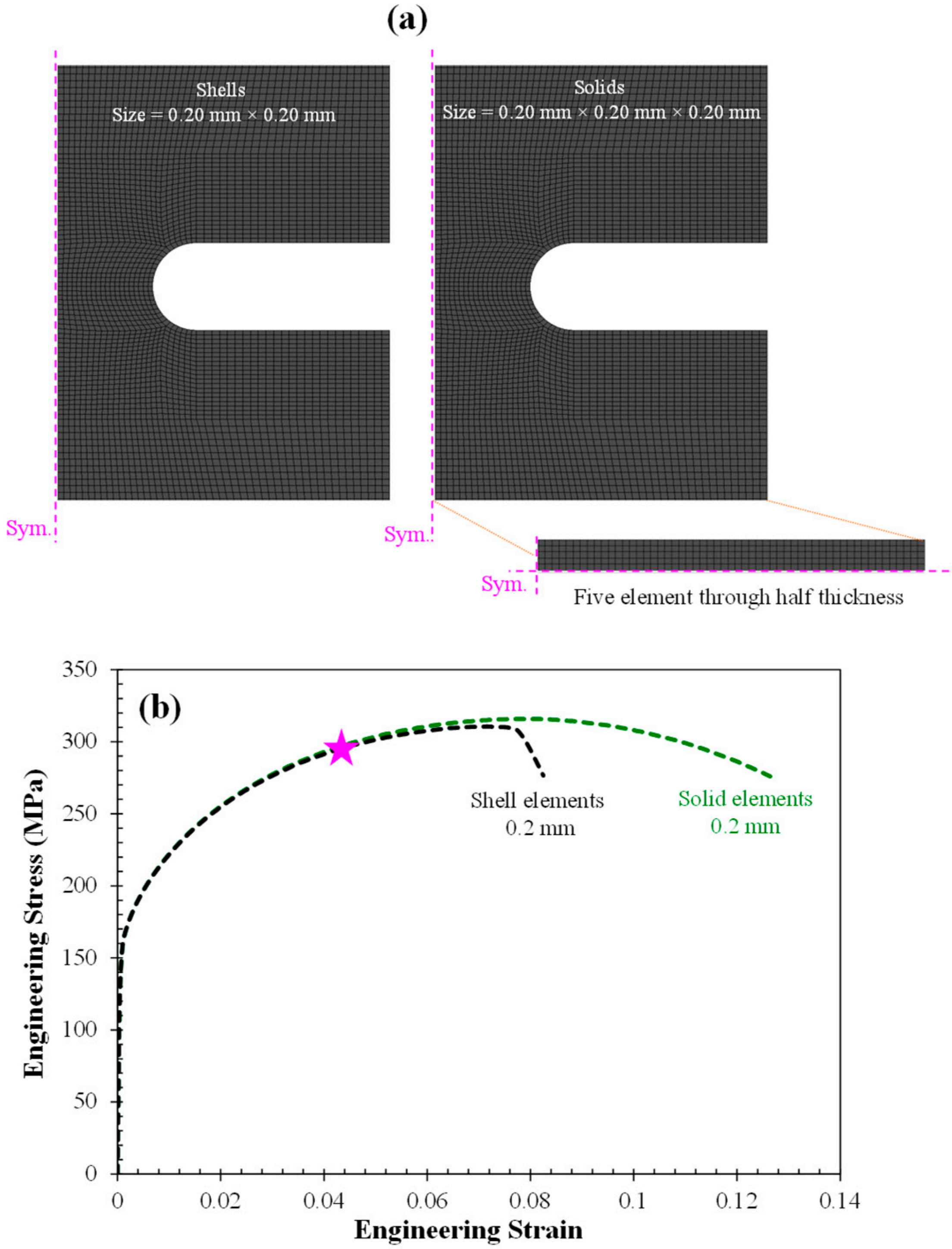

Figure A1. (**a**) Discretized models with shell and solid elements, and (**b**) engineering stress-strain curves obtained from the models. The symbol shows the cut-off for the inverse analysis, based upon when the local element at the notch edge reached the tensile uniform elongation.

Appendix A.2. Effect of Element Size

The influence of element size was considered using shell elements with three different sizes of 0.10 mm, 0.20 mm, and 0.40 mm with an aspect ratio of unity and fully integrated formulation (Type 16 in LS-DYNA), see Figure A2. The three element sizes demonstrated similar engineering stress-strain responses before localization while the local response of the coarser mesh (0.4 mm) was slightly deviated from those of finer meshes. The element size of 0.20 mm appeared small enough to resolve global and local responses of the material before localization.

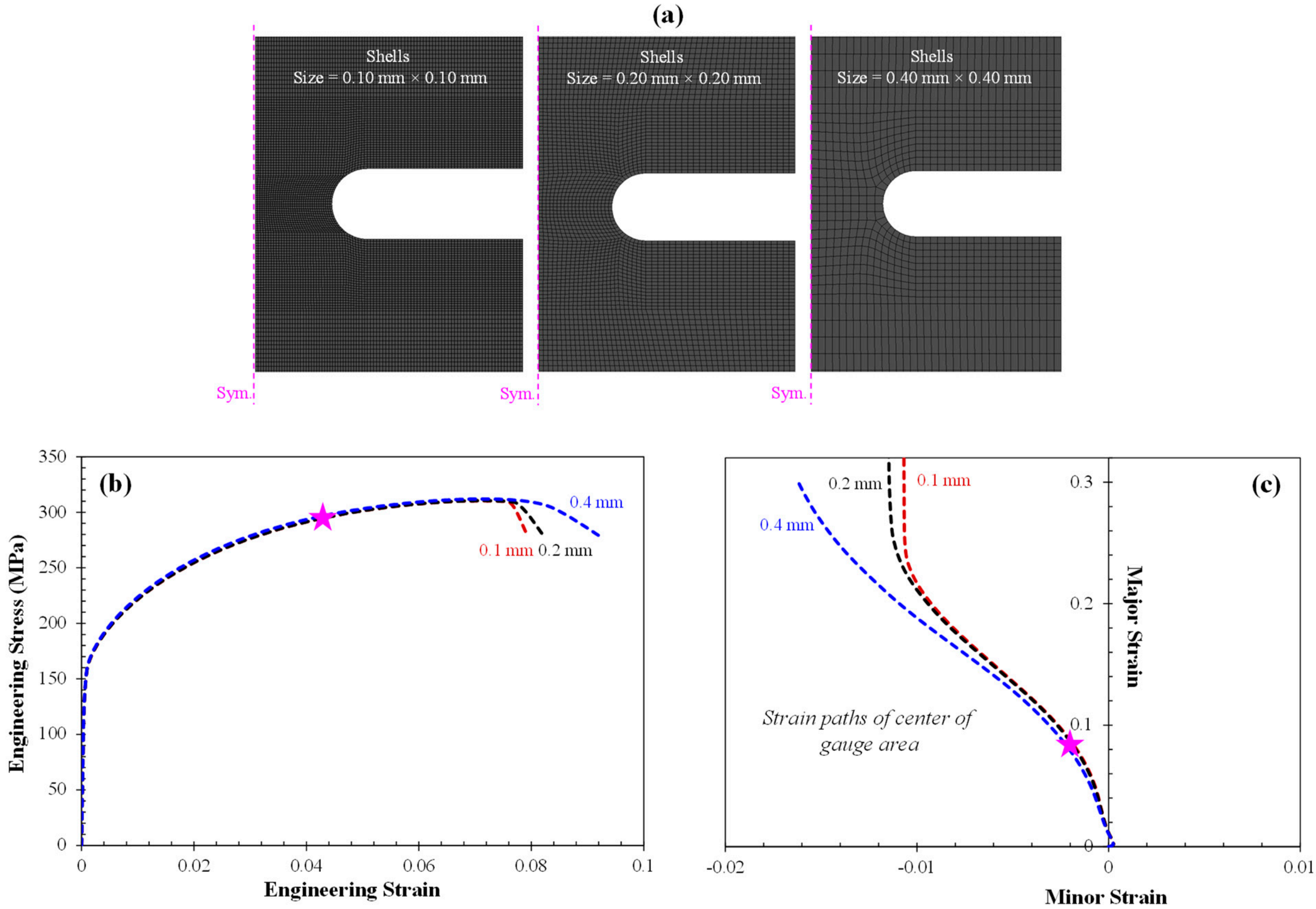

Figure A2. (**a**) Discretized models with shell elements of different sizes, and (**b**) engineering stress-strain curves, and (**c**) local strain paths at the center of the gauge region obtained from the models. The symbol shows the cut-off for the inverse analysis, based upon when the local element at the notch edge reached the tensile uniform elongation.

Appendix A.3. Effect of Element Aspect Ratio

The influence of element aspect ratio was assessed by using three deferent aspect ratios of 0.5, 1.0, and 2.0, while keeping the element area fixed at approximately 0.2×0.2 mm^2 (Figure A3). Fully integrated shell elements were utilized for these simulations. As shown in Figure A3, the element aspect ratio did not affect the global and local responses before the onset of localization. The aspect ratio of unity was employed for the finite-element simulations presented in this paper.

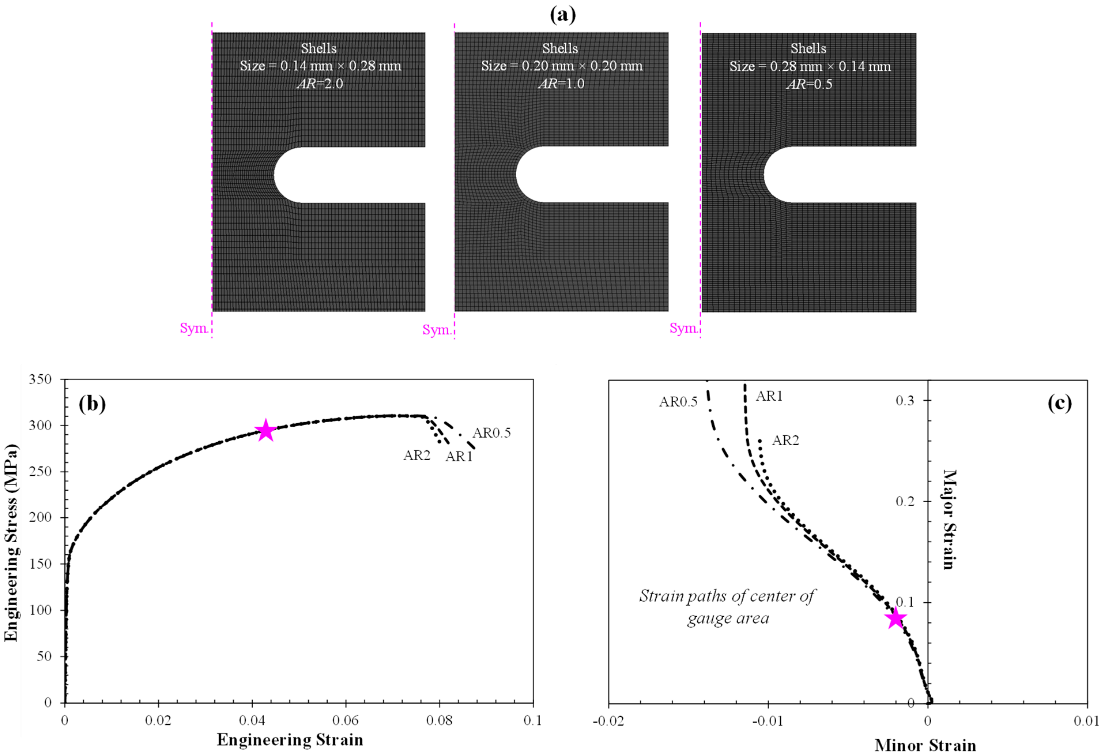

Figure A3. (**a**) Discretized models with shell elements of different aspect ratios, and (**b**) engineering stress-strain curves, and (**c**) local strain paths at the center of gauge region obtained from the models. The symbol shows the cut-off for the inverse analysis, based upon when the local element at the notch edge reached the tensile uniform elongation.

Appendix A.4. Effect of Shell Element Formulation

Two different element formulations were evaluated for the plane stress shell elements: Belytschko-Tsay and fully integrated shell elements corresponding to Types 2 and 16 in LS-DYNA, respectively. The fully integrated element is appropriate for applications where through-thickness deformation is important. Despite the different formulations, Figure A4 demonstrates that the divergence between the results of the models was marginal before localization for the plane strain notch tests. The fully integrated Type 16 element was adopted in this study as it is the common element formulation used in forming and crash applications.

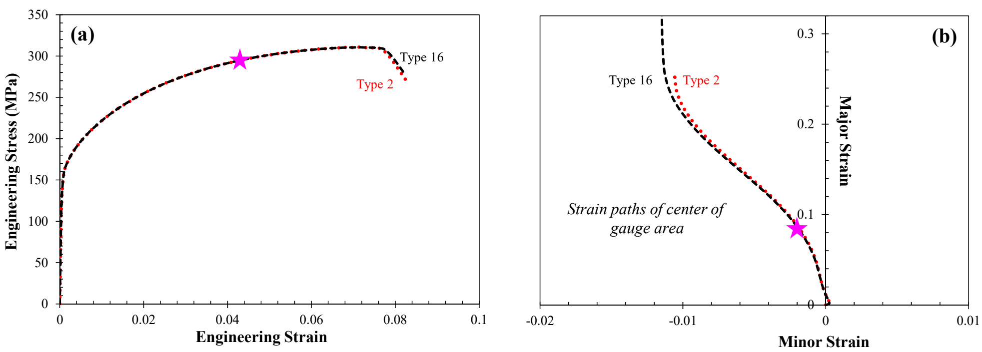

Figure A4. (**a**) Engineering stress-strain curves, and (**b**) local strain paths at the center of gauge region obtained from the models with shell elements and different formulations. The symbol shows the cut-off for the inverse analysis, based upon when the local element at the notch edge reached the tensile uniform elongation.

In summary, the mesh sensitivity analysis in this section confirmed that the selected mesh element size of 0.20 mm with fully integrated formulation and aspect ratio of unity was appropriate for the proposed inverse analysis of plane strain notch tests until the onset of diffuse localization.

References

1. Mahmudi, R. A novel technique for plane-strain tension testing of sheet metals. *J. Mater. Processing Technol.* **1999**, *86*, 237–244. [CrossRef]
2. Wagoner, R.H. Measurement and analysis of plane-strain work hardening. *Metall. Trans. A* **1980**, *11*, 165–175. [CrossRef]
3. Vegter, H.; ten Horn, C.; An, Y.; Atzema, E.H.; Pijlman, H.H.; van den Boogaard, A.H.; Huetink, H. Characterization and modelling of the plastic material behaviour and its application in sheet metal forming simulation. In Proceedings of the VII International Conference on Computational Plasticity, Barcelona, Spain, 7–10 April 2003.
4. An, Y.G.; Vegter, H.; Elliot, L. A novel and simple method for the measurement of plane strain work hardening. *J. Mater. Processing Technol.* **2004**, *155*, 1616–1622. [CrossRef]
5. Flores, P.; Tuninetti, V.; Gilles, G.; Gonry, P.; Duchene, L.; Habraken, A.M. Accurate stress computation in plane strain tensile tests for sheet metal using experimental data. *J. Mater. Processing Technol.* **2010**, *210*, 1772–1779. [CrossRef]
6. Aydin, M.S.; Gerlach, J.; Kessler, L.; Tekkaya, A.E. Yield *locus*evolution and constitutive parameter identification using plane strain tension and tensile tests. *J. Mater. Processing Technol.* **2011**, *211*, 1957–1964. [CrossRef]
7. Tian, H.; Brownell, B.; Baral, M.; Korkolis, Y.P. Earing in cup-drawing of anisotropic Al-6022-T4 sheet. *Int. J. Mater. Form.* **2016**, *10*, 329–343. [CrossRef]
8. Baral, M.; Ha, J.; Korkolis, Y.P. Plasticity and ductile fracture modeling of an Al-Si-Mg die-cast alloy. *Int. J. Fract.* **2019**, *216*, 101–121. [CrossRef]
9. Butcher, C.; Abedini, A. On anisotropic plasticity models using linear transformations on the deviatoric stress: Physical constraints on plastic flow in generalized plane strain. *Int. J. Mech. Sci.* **2019**, *161*, 105044. [CrossRef]
10. Barlat, F.; Lege, D.J.; Brem, J. A six-component yield function for anisotropic materials. *Int. J. Plast.* **1991**, *7*, 693–712. [CrossRef]
11. Barlat, F.; Brem, J.C.; Yoon, J.W.; Chung, K.; Dick, R.E.; Lege, D.J.; Pourboghrat, F.; Choi, S.H.; Chu, E. Plane stress yield function for aluminum alloy sheets—Part I: Theory. *Int. J. Plast.* **2003**, *21*, 1009–1039. [CrossRef]
12. Barlat, F.; Aretz, H.; Yoon, J.W.; Karabin, M.E.; Brem, J.C.; Dick, R.E. Linear transformation-based anisotropic yield functions. *Int. J. Plast.* **2005**, *21*, 1009–1039. [CrossRef]
13. Fast-Irvine, C.; Abedini, A.; Noder, J.; Butcher, C. An experimental methodology to characterize the plasticity of sheet metals from uniaxial to plane strain tension. *Exp. Mech.* **2021**, *61*, 1381–1404. [CrossRef]
14. Hosford, W.F. Comments on anisotropic yield criteria. *Int. J. Mech. Sci.* **1985**, *27*, 423–4270. [CrossRef]
15. Dunand, M.; Mohr, D. Hybrid experimental-numerical analysis for basic ductile fracture experiments for sheet metals. *Int. J. Solids Struct.* **2010**, *47*, 1130–1143. [CrossRef]
16. Marth, S.; Haggblad, H.; Oldenbur, M.; Ostlund, R. Post necking characterization for sheet metal materials using full field measurement. *J. Mater. Processing Technol.* **2016**, *238*, 315–324. [CrossRef]
17. Abedini, A.; Butcher, C.; Worswick, M.J. Application of an evolving non-associative anisotropic asymmetric plasticity model for a rare-earth magnesium alloy. *Metals* **2018**, *8*, 1013. [CrossRef]
18. Ha, J.; Baral, M.; Korkolis, Y.P. Ductile fracture of an aluminum sheet under proportional loading. *Int. J. Mech. Phys. Mater.* **2019**, *132*, 103685. [CrossRef]
19. Lattanzi, A.; Barlat, F.; Pierron, F.; Marek, A.; Rossi, M. Inverse identification strategies for the characterization of transformation-based anisotropic plasticity models with the non-linear VFM. *Int. J. Mech. Sci.* **2020**, *173*, 105422. [CrossRef]
20. Abedini, A.; Narayanan, A.; Butcher, C. An investigation into the characterization of the hardening response sheet metals using tensile and shear tests with surface strain measurement. *Forces Mech.* **2022**, *7*, 10090. [CrossRef]
21. Narayanan, A.; Bourque, C.; Fast-Irvine, C.; Abedini, A.; Anderson, D.; Butcher, C. *Identification of the Plane Strain Yield Strength of Anisotropic Sheet Metals Using Inverse Analysis of Notch Tests*; SAE Technical Paper; SAE International: Warrendale, PA, USA, 2022. [CrossRef]
22. Vegter, H.; van den Boogaard, A.H. A plane stress yield function for anisotropic sheet material by interpolation of biaxial stress states. *Int. J. Plast.* **2006**, *22*, 557–580. [CrossRef]
23. Abedini, A.; Noder, J.; Kohar, C.P.; Butcher, C. Accounting for shear anisotropy and material frame rotation on the constitutive characterization of automotive alloys using simple shear tests. *Mech. Mater.* **2020**, *148*, 103419. [CrossRef]
24. Roth, C.C.; Mohr, D. Ductile fracture experiments with locally proportional loading histories. *Int. J. Plast.* **2016**, *79*, 328–354. [CrossRef]
25. Safaei, M.; Zang, S.; Lee, M.; Waele, W.D. Evaluation of anisotropic constitutive models: Mixed anisotropic hardening and non-associated flow rule approach. *Int. J. Mech. Sci.* **2013**, *73*, 53–68. [CrossRef]
26. Dick, R.E.; Yoon, J.W. Plastic anisotropy and failure in thin metal: Material characterization and fracture prediction with an advanced constitutive model and polar EPS (effective plastic strain) fracture diagram for AA3014-H19. *Int. J. Solids Struct.* **2018**, *151*, 195–213. [CrossRef]

27. Park, N.; Stoughton, T.B.; Yoon, J.W. A criterion for general description of anisotropic hardening considering strength differentia effect with non-associated flow rule. *Int. J. Plast.* **2019**, *121*, 76–100. [CrossRef]
28. Kim, W.; Stoughton, T.B.; Lee, M. Identification of strain localization-induced failure in hot-rolled steel sheets: A hybrid numerical-experimental approach to the virtual forming limit test. *Int. J. Mech. Sci.* **2021**, *193*, 106146. [CrossRef]
29. Abedini, A.; Butcher, C.; Nemcko, M.J.; Kurukuri, S.; Worswick, M.J. Constitutive characterization of a rate-earth magnesium alloy sheet (ZEK100-O) in shear loading: Studies of anisotropy and rate sensitivity. *Int. J. Mech. Sci.* **2017**, *128*, 54–69. [CrossRef]
30. Abedini, A.; Butcher, C.; Rahmaan, T.; Worswick, M.J. Evaluation and calibration of anisotropic yield criteria in shear loading: Constraints to eliminate numerical artefacts. *Int. J. Solids Struct.* **2018**, *151*, 118–134. [CrossRef]
31. Bai, Y.; Wierzbicki, T. Application of extended Mohr-Coulomb criterion to ductile fracture. *Int. J. Fract.* **2010**, *161*, 1. [CrossRef]
32. Mohr, D.; Marcadet, S. Micromechanically-motivated phenomenological Hosford-Coulomb model for predicting ductile fracture initiation at low stress triaxialities. *Int. J. Solids Struct.* **2015**, *67*, 40–55. [CrossRef]
33. Kuwabara, T.; Tachibana, R.; Takada, Y.; Koizumi, T.; Coppieters, S.; Barlat, F. Effect of hydrostatic stress on the strength differential effect in low-carbon steel sheet. *Int. J. Mater. Form.* **2022**, *15*, 13. [CrossRef]
34. Hosford, W.F. A generalized isotropic yield criterion. *J. Appl. Mech.* **1972**, *39*, 607–609. [CrossRef]
35. Hockett, J.E.; Sherby, O.D. Large strain deformation of polycrystalline metals to low homologous temperatures. *J. Mech. Phys. Solids* **1975**, *23*, 87–98. [CrossRef]
36. Noder, J.; Butcher, C. A comparative investigation into the influence of the constitutive model on the prediction of in-plane formability for Nakazima and Marciniak tests. *Int. J. Mech. Sci.* **2019**, *165*, 105138. [CrossRef]
37. Swift, H.W. Plastic instability under plane stress. *J. Mech. Phys. Solids* **1952**, *1*, 1–18. [CrossRef]
38. Abspoel, M.; Scholting, M.E.; Lansbergen, M.; An, Y.; Vegter, H. A new method for prediction advanced yield criteria input parameters from mechanical properties. *J. Mater. Processing Technol.* **2017**, *248*, 161–177. [CrossRef]
39. Suh, Y.S.; Saunders, F.I.; Wagoner, R.H. Anisotropic yield functions with plastic-strain-induced anisotropy. *Int. J. Plast.* **1996**, *12*, 417–438. [CrossRef]
40. Hill, R. Theoretical plasticity of textured aggregates, theory of the yielding and plastic flow of anisotropic metals. *Math. Proc. Camb. Philos. Soc.* **1979**, *85*, 179–191. [CrossRef]
41. Iniguez-Macedo, S.; Lostado-Lorza, R.; Escribano-Garcia, R.; Martinez-Calvo, M.A. Finite element model updating combined with multi-response optimization for hyper-elastic materials characterization. *Materials* **2019**, *12*, 1019. [CrossRef] [PubMed]